Templates of Expected Measurement Uncertainties: a CSEWG Effort,
Cyrille De Saint Jean and Denise Neudecker (Guest editors)

EPJ Nuclear Sciences & Technologies

REGULAR ARTICLE

OPEN ⧉ ACCESS

Templates of expected measurement uncertainties for neutron-induced capture and charged-particle production cross section observables

Amanda M. Lewis[1,*] ⓘ, Denise Neudecker[2], Allan D. Carlson[3], Donald L. Smith[4], Ian Thompson[5], Anton Wallner[6,7], Devin P. Barry[1], Lee A. Bernstein[8,9], Robert C. Block[10], Stephen Croft[11], Yaron Danon[10], Manfred Drosg[12], Robert C. Haight[2], Michal W. Herman[2], Hye Young Lee[2], Naohiko Otuka[13], Henrik Sjöstrand[14], and Vladimir Sobes[15]

[1] Naval Nuclear Laboratory, Schenectady, NY 12301-1072, USA
[2] Los Alamos National Laboratory, Los Alamos, NM 87545, USA
[3] National Institute of Standards and Technology, Gaithersburg, MD 20899-8463, USA
[4] Argonne National Laboratory, Argonne, IL 60439-4842, USA *(retired)*
[5] Lawrence Livermore National Laboratory, Livermore, CA 94551-0808, USA
[6] Helmholtz Centre Dresden Rossendorf, 01328 Dresden, Germany
[7] The Australian National University, Canberra, ACT 0200, Australia
[8] University of California Berkeley, Berkeley, CA 94720, USA
[9] Lawrence Berkeley National Laboratory, Berkeley, CA 94720, USA
[10] Rensselaer Polytechnic Institute, Troy, NY 12180, USA
[11] Lancaster University, Lancaster LA1 4YW, UK
[12] University of Vienna, 1010 Vienna, Austria
[13] International Atomic Energy Agency, 1400 Vienna, Austria
[14] Uppsala University, 75120 Uppsala, Sweden
[15] University of Tennessee, Knoxville, TN 37996, USA

Abstract. This paper provides a template of expected uncertainties and correlations for measurements of neutron-induced capture and charged-particle production cross sections. Measurements performed in-beam include total absorption spectroscopy, total energy detection, γ-ray spectroscopy, and direct charged-particle detection. Offline measurements include activation analysis and accelerator mass spectrometry. The information needed for proper use of the datasets in resonance region and high energy region evaluations is described, and recommended uncertainties are provided when specific values are not available for a dataset.

1 Introduction

Neutron-induced capture and charged-particle production reactions are important for accurate modeling of many systems, including nuclear reactors [1,2], astrophysical environments [3–5], and neutron activation analysis [6,7]. Cross sections and outgoing particle spectra are evaluated based on available experimental datasets, which in many cases use different measurement methods. Comparing data quality across different measurement types requires that evaluators have a basic understanding of the experiments and a reasonable method for estimating uncertainties that can be applied consistently. As explained in the opening paper [8] of this topical issue on templates of expected measurement uncertainties, the purpose of this work and the other works in the issue is to provide templates for various neutron-induced reaction observables. The templates list common measurement techniques and applicable uncertainty sources for particular observables and recommended conservative values if insufficient information is provided by the authors. Complete uncertainty estimation for datasets in an evaluation can have a significant effect on the final evaluated values and uncertainties [8,9], so the estimates must be reasonable and consistent.

This work provides a template for neutron-induced capture and charged-particle production reactions that can be measured by the detection of one or more of the light reaction products from an in-beam sample (at the time the reaction is occurring) or the product nucleus by decay or mass spectroscopy offline (after the irradiation has ended). Offline measurements of the product

* e-mail: amandalewis@lbl.gov

nucleus are the most specific measurements of an exclusive cross-section (defined by a unique product nucleus) but are only possible when the product nucleus has certain characteristics that allow it to be fully quantified after the irradiation for time-integrated results. In-beam measurements of lighter reaction products allow for the measurement of reactions with stable product nuclei and can provide Time-of-Flight (TOF) (and therefore neutron-energy) dependent cross sections, but the efficiency and backgrounds must be well-characterized to ensure that only the reaction of interest contributes to the final measurement results. Both TOF and mono-energetic (or quasi-mono-energetic) measurements are covered here.

A high-level description of the measurement types considered in this template is given in Section 2, where Section 2.2 covers the in-beam measurement types (total absorption spectroscopy, total energy detection, γ-ray spectroscopy measurements, and direct charged-particle measurements) and Section 2.3 covers the offline measurement types (activation analysis and accelerator mass spectroscopy). The information needed for evaluations is discussed in Section 3 for Resolved Resonance Region (RRR), Unresolved Resonance Region (URR), and High Energy Region (HER) evaluations. The template of expected measurement uncertainties and correlations is presented in Section 4. The basic sources of uncertainty included are neutron production and quantification, counting statistics, backgrounds, sample characteristics, detector and system efficiencies, and resolution functions. Earlier versions of the capture measurement types and template were originally reported in the dissertation of the first author [10].

2 Measurement types

Capture and charged-particle production reaction cross-section measurements are split into two basic categories–in-beam and offline–based on how the reaction yield is determined. However, there are similarities between these measurement types which are covered in Section 2.1, followed by specifics of in-beam measurements in Section 2.2 and offline measurements in Section 2.3.

2.1 Common characteristics

The characteristics of the measurement types are split into six basic categories – the Facilities and setup used, the important Sample Characteristics, the Efficiency components and calibration, the Background sources and procedures, the Flux Determination and/or Normalization, and the Data Analysis inputs and equations. These six categories are used to describe each of the measurement types, allowing for straightforward comparisons of the different methods. This Section describes the categories in general, and is referenced in the following sections describing specifics about the measurement types.

Facilities. The various measurement types use many different neutron sources and detection systems, which are explained here.

White neutron sources can be used with in-beam measurement types to determine neutron energy-differential yields or cross sections and with offline measurement types to determine spectrum-averaged cross sections, such as Maxwellian Averaged Cross Sections (MACS), which are used in modeling astrophysical nucleosynthesis.

Mono-energetic and thermal-spectrum neutron sources are likewise used with both in-beam and offline measurement types. Reactors can be used to perform measurements in a thermal spectrum, such as at the Budapest Research Reactor [6]. For HER measurements, reactions such as $D(d,n)^3He$ [11–14], $T(p,n)^3He$ [15,16], $T(d,n)^4He$ [11], $^7Li(p,n)$ [17,18], and even $^{18}O(p,n)$ [3] can be used. The Associated Particle (AP) technique [19] is often used to quantify the neutron flux for in-beam measurements, where the detection of the charged-particle product of the neutron-production reaction acts as a trigger to record the signal from any reactions that occur. The fluence, Φ, which is the time-integrated flux of the irradiation, can also be determined by this method for offline measurements [20]. The measurement of the associated charged-particle is itself an in-beam direct charged-particle detection measurement as described in Section 2.2.4.

The detection systems used vary from an individual detector in a low-background room to large detector arrays installed at accelerator facilities. For γ-ray detectors, the energy resolution, timing resolution, and sensitivity to neutrons are important factors. For charged-particle detectors, important factors include intrinsic efficiency, energy and angle resolution, and sensitivity to all backgrounds.

Sample characteristics. For capture and charged-particle production reaction measurements, the sample is typically thin to minimize neutron multiple scattering and attenuation of the reaction products.

Sample non-uniformity is an important consideration for direct charged-particle measurements, where even small variations can have significant impacts on the energy of the exiting particle.

The size of the sample in relation to the diameter of the incident beam is important for determining the correct number density value to use in the calculation. An overfilled sample, where the beam is larger than the sample (shown in Fig. 1a) will be irradiated in its entirety and the sample mass and spatial distribution of the beam are important for determining the effective number density. An underfilled sample, where the beam spot is smaller than the sample (shown in Fig. 1b) will only be irradiated where the beam spot is and the sample areal density and the beam spot size are used to determine the effective number density. The correction for the beam-sample spatial overlap, referred to as the Beam Interception Factor [21], $\oslash$, can be very precise for a smooth sample of uniform thickness and a well-characterized beam spot.

Efficiency. The efficiency of measurement determines how many real events are correctly detected and counted. The intrinsic and geometric efficiency of the detector system, coincidence triggers, and cuts or thresholds in
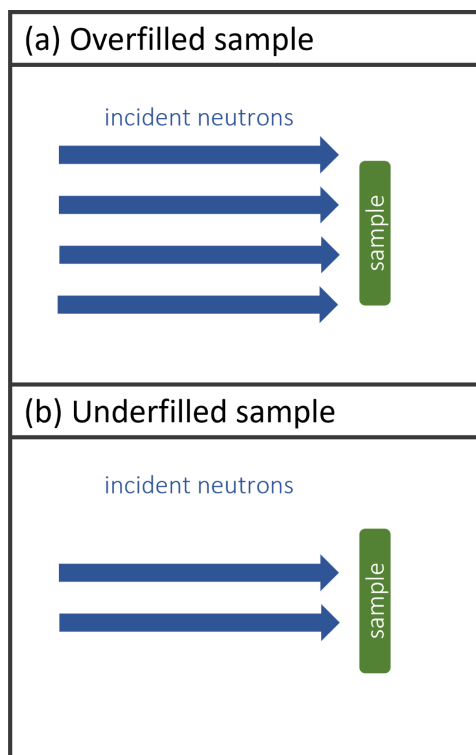
Fig. 1. Schematics of the beam-sample spatial overlap, known as the Beam Interception Factor. (a) Shows an overfilled sample, which is smaller than the beam spot. (b) Shows an underfilled sample, which is larger than the beam spot.

the data analysis all contribute to the overall system efficiency. The detector efficiency can often be quantified by measurement, sometimes supplemented by simulations for interpolation or extrapolation. The effect of triggers and thresholds on the system efficiency can be more complicated, requiring the estimation of how many events are excluded.

Backgrounds. The background sources discussed for each measurement type are characterized by whether they are dependent on the incident neutron energy, and whether they are dependent on the sample used in the measurement. Backgrounds that are independent of both energy and sample include the room background and electronic noise. Sample-independent backgrounds that are dependent on neutron energy include γ rays and charged particles from an accelerator and neutrons scattered by the detector setup. Backgrounds that are sample-dependent but independent of neutron energy are those from isotopes that are in the sample prior to irradiation, such as radioactive samples. Those that are both sample and energy-dependent include signals from neutrons and γ rays scattered by the sample and from other reactions caused by the irradiation, and Compton scattering backgrounds in high-resolution γ-ray detectors such as HPGe.

Some backgrounds can be determined by measurement, such as by measuring without the sample or without the neutron source, while others are modeled. Background

corrections can be performed by subtraction, suppression, or incorporation into the experiment model.

In many cases, the backgrounds are not explicitly represented in data analysis equations, such as when they are implicitly included in "background-corrected" counts or when suppression was performed rather than subtraction. In the case of resonance region capture yield measurements with white neutron sources, the measured background sources are explicitly treated and can generally be split up into three components [22],

$$\dot{B}(t) = \dot{B}_0 + \dot{B}_{\mathrm{OB}}(t) + \dot{B}_S(t), \tag{1}$$

where $\dot{B}_0$ represents the sample- and time-independent background count rate, $\dot{B}_{\mathrm{OB}}(t)$ is the background count rate from γ-ray signals in the room, and $\dot{B}_S(t)$ is the background count rate from γ-rays induced by interactions with the sample. The room background can be characterized with sample-out measurements, and the sample-dependent background is characterized and/or minimized based on the measurement type.

Flux determination and normalization. In resonance region (RRR and URR) white-source measurements, the reaction yield is typically normalized in magnitude to a strong resonance and in shape to a monitor reaction. For thermal spectrum-averaged measurements and in the HER, common methods include using a monitor cross-section, shown in Figure 2a, measurement with a fission chamber, Figure 2b, or using the AP technique, Figure 2c. Monitor reactions are commonly used in offline measurements and provide a measurement of the overall irradiation fluence. In the thermal region, ^{197}Au and ^{94}Zr are common monitors [6,7,23], and in the RRR smooth cross sections like ^{10}B(n,α) and ^{6}Li(n,t) are used [22,24]. Monitor reactions can also be used in the HER, such as ^{56}Fe(n,n') [25]. Direct measurement of the flux with fission chambers [26,27] provides energy-differential flux values for HER TOF measurements, and can be used in thermal measurements as well. Other neutron detectors, such as scintillators and long-counters, are also used.

Data analysis. Direct flux measurement with fission chambers or the AP technique requires reliable reaction cross sections (and outgoing particle angular distributions for AP measurements), which usually come from evaluated libraries such as the ENDF/B-VIII.0 [28], JEFF-3.3 [29], and JENDL-5.0 [30] libraries. Monitor reactions need to have well-characterized cross sections as well, and commonly used reactions can be found in the focused International Reactor Dosimetry and Fusion File (IRDFF) database [31]. For radioactive nuclei measured with activation analysis, the decay data needed include the half-life and the intensities of the decay products measured. Decay and structure data can be found in the Evaluated Nuclear Structure Data File (ENSDF) library [32]. For measurement techniques that involve simulating capture γ-ray cascades, evaluated capture γ-ray intensities are also compiled in ENSDF when available.

For TOF measurements in the resonance region, the measurement observable is the reaction yield, rather than
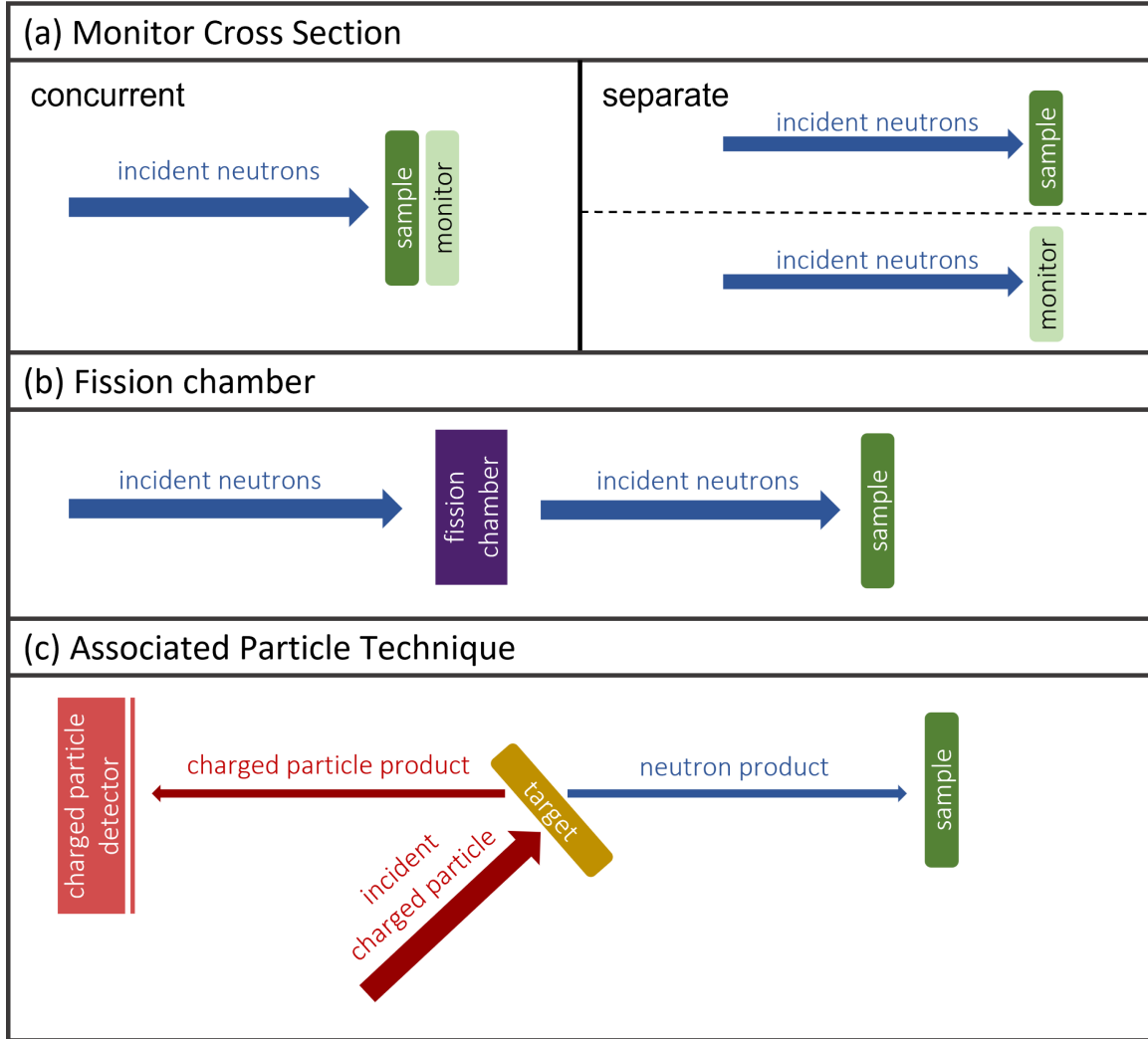
Fig. 2. Schematics of the neutron flux normalization methods used in various measurement types. (a) Shows a monitor cross section, which is a well-known reaction that is irradiated with the sample to determine the flux. (b) Shows direct measurement of the flux with a fission chamber. (c) Shows the Associated Particle technique, where the charged product of a neutron-production reaction is directly measured.

the cross-section. The experimental yield is used directly in the evaluation process, similar to the transmission [33]. The experimental effects that are modeled include Doppler broadening, self-shielding, γ-ray attenuation, and multiple scattering, in addition to other effects in the experimental resolution function. In the URR, the Doppler broadening and self-shielding effects can be quantified in a fluctuation correction factor[1], F_γ. The correction factor F_γ is calculated by modeling the capture yield, Y_γ, for the real sample with number density n, and for a very thin sample with number density n_{thin}, which has no multiple scattering or self-shielding effects. This ratio can be related to the ratio of the measured yield, Y_{exp}, to the theoretical yield, Y_0,

$$F_\gamma = \frac{\langle Y_\gamma(n)\rangle/n}{\langle Y_\gamma(n_{\text{thin}})\rangle/n_{\text{thin}}} = \frac{\langle Y_{\text{exp}}\rangle}{\langle Y_0\rangle}, \tag{2}$$

where Y_0 has no self-shielding or multiple-scattering effects and can be directly related to the average cross-section, $\langle\sigma_\gamma\rangle$,

$$\langle\sigma_\gamma\rangle = \frac{\langle Y_0\rangle}{n} = \frac{\langle Y_{\text{exp}}\rangle/F_\gamma}{n} = \frac{\langle Y_{\text{exp}}\rangle}{F_\gamma n}. \tag{3}$$

The correction is minor for thin samples but can be very large for thicker samples [22].

For measurements with spectrum-averaged or monoenergetic neutron sources, the observable can be the production cross-section of a γ-ray, the angle-differential cross-section of a charged-particle product, or the energy- and angle-integrated reaction cross-section.

---

[1] This correction for a fluctuating cross section is not the same as the Width Fluctuation Correction used in the Hauser-Feshbach formula to account for correlations between incident and outgoing channels [34].
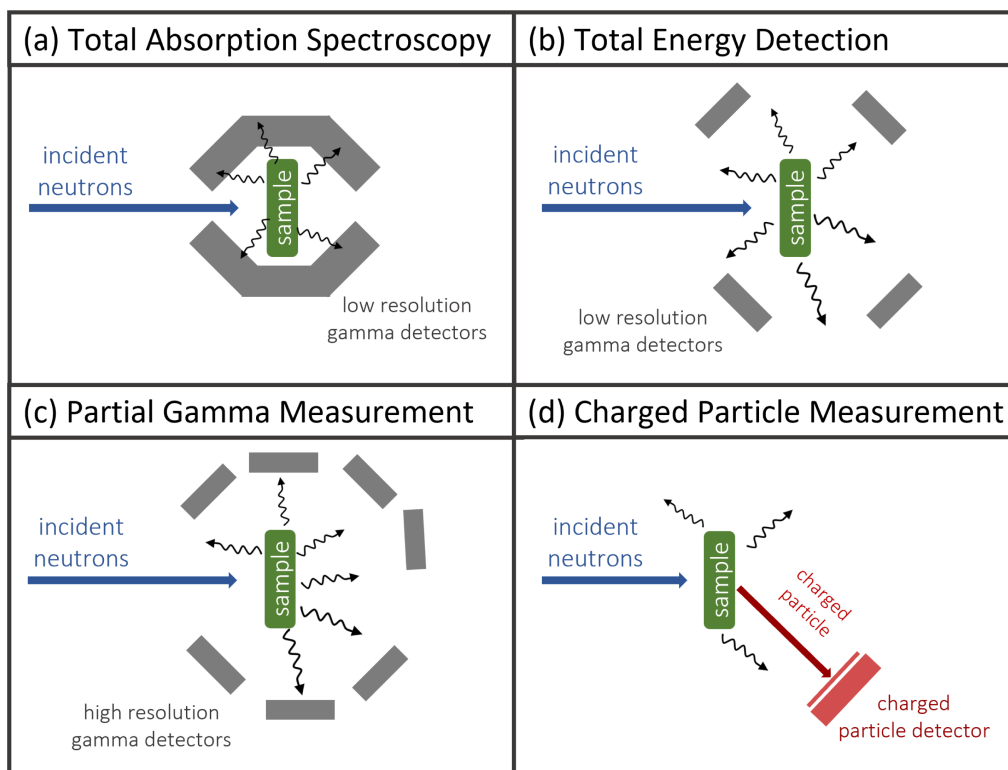
Fig. 3. Schematics for in-beam methods: (a) Total Absorption Spectroscopy, (b) Total Energy Detection, (c) γ-Spectroscopy, and (d) Charged Particle detection.

2.2 Specifics of in-beam measurements

In-beam measurements detect prompt reaction products, usually lighter products rather than the product nucleus. In capture reactions, this is always the emitted γ rays, and for charged-particle reactions, the detected products can be charged particles or emitted γ rays. The four types of in-beam measurements covered here are Total Absorption Spectroscopy (used for capture), Total Energy Detection (used for capture), γ-Spectroscopy measurements (used for capture and charged-particle production), and Charged-Particle detection (used for charged-particle production). Schematics of the measurement types are shown in Figure 3.

2.2.1 Total absorption spectroscopy

Facilities. Total Absorption Spectroscopy (TAS) measurements utilize large solid-angle (nearly 4π coverage) detector systems composed of high-efficiency γ-ray detectors to maximize the energy deposited in the detectors [22]. A schematic of the detector setup for TAS measurements is shown in Figure 3a.

TAS measurements have been performed at facilities such as Rensselaer Polytechnic Institute (RPI) [35], Argonne National Laboratory (ANL) [36], Karlsruhe [37], the Oak Ridge Electron Linear Accelerator (ORELA) [38], the Kyoto University Research Reactor Institute (KURRI) [39,40], the CERN Neutron Time-of-Flight (n_TOF) Facility [41], and the Los Alamos Neutron

Science Center (LANSCE) [42]. Some systems use NaI detectors [35,43] and others use BaF_2 [37,41,44], and the systems are generally composed of many detector segments with separate signals. The detector systems are designed to maximize the efficiency of detecting and identifying the capture γ-ray cascade. These measurements can be done in any energy region, but are uniquely well-suited for measurements in the RRR and URR where fast timing ($\leq 1\,\mathrm{ns}$) is needed to resolve the cross-section structure.

Sample characteristics. Samples used for TAS measurements should be thin to minimize multiple-scattering and γ-ray attenuation, as explained in Section 2.1, but the optimization is not as necessary for TAS measurements as for some measurement types. The modeling used for efficiency determination (explained below) and in the evaluation process (explained in Sect. 3.1) accounts for γ-ray attenuation and neutron multiple-scattering in the experiment analysis. The composition of the sample is important when the measurement method cannot easily distinguish between different reactions.

Efficiency. The quantification of the efficiency to detect a capture event by identifying the capture cascade is a complex process of convolving the physical detector efficiencies (geometric and intrinsic), the characteristics of the cascades, and the thresholds used in the data analysis process. Thresholds used in the data analysis that impose maximum and/or minimum values for energy

deposited in a single segment or in the system and the observed multiplicity of the event can have a large impact on the overall efficiency, and when stringent thresholds are imposed the cascade characteristics can become very important to understand. This is demonstrated in a detailed analysis of the efficiency of the n_TOF Total Absorption Calorimeter [45], in which the physical efficiency is well-characterized using a GEANT-4 [46] model. The sensitivity of the modeled efficiency is studied for three measurements: ^{nat}Ti, for which the main reaction, ^{48}Ti(n, γ), has a well-characterized thermal γ-ray cascade [47], ^{197}Au, for which the studied photon strength function (PSF) models did not greatly impact the modeled efficiency, and ^{240}Pu, for which the studied PSF models did have a large impact on the modeled efficiency. For the case of ^{197}Au, the capture cascade detection efficiency varied from over 97% with no thresholds, to about 31% for a total energy deposited threshold of 4 MeV and an observed multiplicity threshold of 3. Restrictive thresholds are often used to separate the signals for different reactions, such as capture and fission in a fissile nucleus [2,48], or capture in different isotopes in a natural sample [49].

Backgrounds. Observed multiplicity thresholds can be used to suppress background signals, such as energy- and sample-independent signals from radioactive isotopes in the environment [18] or energy- and sample-dependent scattering in the sample and experimental system (neutron sensitivity) [49]. For the Karlsruhe 4π detector, it was estimated that low energy and multiplicity thresholds eliminated about ~50% of the scattered neutron background and only about ~2% of real capture events [50].

The measured energy-dependent background from neutrons scattered on the sample or setup, $\dot{B}_S(t)$ in equation (1), is often measured using "pure scattering" samples such as graphite or lead, which simulate the neutrons scattered from the sample into the detectors. Carbon and lead scattering cross sections are well-known, and the scattering yield can be normalized to that of the measured isotope, but have very different characteristics for scattering γ rays in the environment [44] which can impact the background measurement. For the RPI NaI detector system, capture in ^{127}I was measured using carbon and lead samples and found to be less than 2.5% below 1 keV [2]. For the Karlsruhe BaF$_2$ detector system, neutron capture in ^{135,137}Ba was measured using a graphite sample and normalized to events with deposited energy above 8 MeV in subsequent sample runs [50].

Flux normalization. The number of incident neutrons is needed to normalize the count rate to the absolute capture yield for a sample. One common method for normalization is to use a monitor cross-section which is well-known, such as ^{197}Au(n, γ). The reaction of interest is measured as a ratio to the monitor cross section at each incident neutron energy, with various corrections applied to account for the differences between the samples, reaction characteristics, and γ-ray cascades.

Another method to normalize the count rate to absolute capture yield is the "saturated resonance" technique, which is also used in transmission measurements for background characterization [33]. A saturated resonance will capture or scatter nearly all neutrons, so the yield can be normalized to the ratio of the capture cross-section to the total cross-section. Saturated resonances that are dominated by capture are usually chosen, so the capture-to-total ratio is nearly one. A saturated resonance in the isotope is typically used when possible. This method requires fewer corrections, as it is only assumed that the efficiency for detecting capture cascades is the same for different resonances in the same isotope. For measurements without any saturated resonances in the isotope being measured, the normalization can also be done by the simultaneous fitting of transmission and capturing yield data at lower energies [51] or using a saturated resonance in another isotope with appropriate efficiency corrections applied [52,53].

Data analysis. The factors in the ratio normalization are explicitly stated in reference [50], where the capture cross-section of the measured isotope "X" at neutron energy, E_n, $\sigma_X(E_n)$, is:

$$\sigma_X(E_n) = \sigma_{Au}(E_n) \times \frac{Y_X(E_n)}{Y_{Au}(E_n)} \times \frac{\sum_N Y_{Au}}{\sum_N Y_X}$$
$$\times \frac{\sum_E Y_X}{\sum_E Y_{Au}} \times \frac{d_{Au}}{d_X} \times F_1 \times F_2. \tag{4}$$

In this equation, $Y(E_n)$ is the background-corrected count rate at neutron energy E_n, and d represents the sample thickness in units of atoms/barn. The sum terms, $\sum_N Y$ and $\sum_E Y$, are over the regions used for normalization in the TOF spectrum and the total energy deposited, respectively. The region used in the TOF spectrum was optimized for the facility to reduce the ^{135,137}Ba capture background signal and the region used in the energy deposited spectrum was optimized for each sample.

Finally, the ratios of capture events below the energy deposited threshold, F_1, and for multiple scattering in the samples, F_2, must be determined. In reference [50], for BaF$_2$ detectors, the calculated fraction of events below the threshold is highly dependent on the threshold values and efficiency modeling assumptions and ranged from 1.5% to 12%. The correction factor F_1, which is the ratio for each sample studied to ^{197}Au, however, was found to be less than 2% as the calculations were more sensitive to the threshold values than the isotope characteristics. Later measurements at the Karlsruhe detector system used cascade characteristics derived directly from measured data, leading to F_1 correction ratios of about 5% for ^{151}Sm at the energy deposited thresholds of 1.7–1.8 MeV [54], and about 1% for ^{141}Pr and between 1 and 5% for $^{160-164}$Dy relative to ^{197}Au at the presumed energy deposited threshold of 1.8 MeV [55]. When used with low energy thresholds, the high overall efficiency minimizes the sensitivity to cascade modeling uncertainties. When more restrictive thresholds are used the overall cascade efficiency can be much lower. For ^{70,72}Ge measured with the Detector for Advanced Neutron Capture Experiments (DANCE) [56] at LANSCE, minimum thresholds of 5.5 and 4.5 MeV lead

to efficiencies of about 50% and 57% [49]. Calculations provided in the paper show that for both isotopes, the efficiency falls below 20% within 0.5 MeV of the reaction Q-value.

2.2.2 Total energy detection

Facilities. While TAS measurements aim to reduce sensitivity to the capture cascade characteristics by maximizing efficiency, Total Energy Detection (TED) measurements utilize a low-efficiency detector system. The detectors used in TED measurements typically have poor γ-ray energy resolution, as they are optimized for timing resolution to resolve structure in the RRR and URR. TED measurements rely on creating a detector system for which the efficiency to detect a single γ ray is low and proportional to the γ-ray energy–if so, the efficiency to detect a cascade is proportional to the Q-value of the capture reaction [22]. A schematic of a TED detector setup is shown in Figure 3b.

C_6D_6 detector systems have been used at many facilities, including RPI [24], the Geel Electron LINear Accelerator (GELINA) [57], CERN [58], KURRI [59], and ORELA [60], and NaI systems have been used at J-PARC [61].

Sample characteristics. Thin samples are used to minimize multiple scattering and γ-ray attenuation, but these effects can be modeled for thicker samples, as explained in Section 2.2.1. Some measurements utilize thick samples specifically to validate such modeling [62]. Sample composition is important for TED measurements, as there is no way to use characteristic γ rays or total energy deposition thresholds to identify the signal from other reactions occurring in the sample.

Efficiency. The original TED systems, known as Moxon-Rae detectors [63], achieved this proportionality intrinsically for γ-ray energies above 1 MeV but had extremely low detection efficiencies and have generally been replaced with C_6D_6 systems. As the intrinsic efficiency of C_6D_6 detectors is not proportional to the γ-ray energy, the needed detector system efficiency is constructed in the data analysis using the Pulse Height Weighting Technique (PHWT) [64]. The weighting function converts the true system efficiency, using model simulations of the capture cascade and γ-ray transport within the detector system, to the desired $\epsilon_\gamma \propto E_\gamma$ dependence. More details about the development and validation of the PHWT can be found in reference [22]. TED measurements do not use the total energy and multiplicity thresholds used in TAS measurements, but do impose thresholds on the minimum energy deposited in a single detector. This threshold is accounted for in the weighting function and the corresponding correction is dependent on the cascade model used [22].

Backgrounds. The time-dependent background from neutron capture events in the detector material can be measured using a "pure scattering" sample and subtracted using equation (1), as is done in TAS measurements [22].

The characteristics of the scattering sample should be as similar to the sample being measured as possible, as both the scattered neutrons and γ rays contribute to this background [44].

A new background suppression method has been developed, called "i-TED," which uses spatial imaging to discriminate between capture events occurring in the sample and in the detector system itself [65]. Measurements of two well-characterized reactions, $^{197}\mathrm{Au}(n,\gamma)$ and $^{56}\mathrm{Fe}(n,\gamma)$, show that significant suppression can be obtained with the additional spatial cuts, but at the cost of reduced efficiency [66].

Flux normalization. Normalization of the count rates into capture yields is similar to TAS measurements, often using a saturated resonance in the isotope being measured [24] or in $^{197}\mathrm{Au}$ [67], or by simultaneous fitting of transmission and capture yield data [51].

Data analysis. When a monitor material such as $^{10}\mathrm{B}$ is used to measure the flux shape, the yield is determined by a ratio of the weighted count rate for the sample, $\dot{c}_i$, to that of the reference material, $\dot{c}_\phi$,

$$Y_{\mathrm{exp}} = N_\gamma \frac{\dot{c}_i - \dot{B}_i}{\dot{c}_\phi - \dot{B}_\phi} Y_\phi, \qquad (5)$$

where $\dot{B}_i$ and $\dot{B}_\phi$ are the background count rates for the sample and the reference material, respectively. N_γ is the flux normalization factor, and Y_ϕ is the normalized yield to a saturated resonance.

2.2.3 γ-ray spectroscopy measurement

Facilities. The use of high-resolution γ-ray detectors such as Ge(Li) or HPGe can simplify the background compared to TAS and TED measurements. Any number of high-resolution detectors surrounding a sample allows for the identification of discrete γ rays that are characteristic of the product nucleus of the reaction, and can therefore be used for capture and charged-particle production reaction cross-section measurements. A simple schematic of a γ-ray spectroscopy measurement is shown in Figure 3c.

This method relies on high γ-energy resolution detectors which cannot match the timing resolution of the TAS and TED detectors, and it is often employed in spectrum-averaged (thermal or Maxwellian) measurements and in the HER rather than RRR measurements. High-resolution measurements of capture γ-ray spectra under resonances, performed at reactor facilities such as the High Flux Beam Reactor at Brookhaven National Laboratory [68] and accelerator facilities such as the Joint Institute of Nuclear Research at Dubna [69], usually focused on and reported structure information rather than capture yields.

Thermal capture cross sections are often measured at reactor facilities, including two large measurement campaigns involving many samples undertaken at the Budapest Reactor [6,70], which is the basis of the Evaluated γ-ray Activation File (EGAF) database [71], and at the BR1 reactor at SCK-CEN [72]. In the HER, γ-ray spectroscopy was used to measure numerous cross sections, including capture and charged-particle

production reactions, with the GEANIE spectrometer at LANSCE [26].

Sample characteristics. Thin samples are used to minimize neutron multiple scattering, which needs to be corrected (rather than forward-modeled) in HER measurements. The effects of γ-ray attenuation can be calculated for each discrete γ ray if the sample is thick enough to require such a correction.

Efficiency. The detectors used in γ-ray spectroscopy measurements have low intrinsic efficiencies which can be determined with decay calibration sources. Such calibration sources are common for γ-ray energies below 2.6 MeV but for higher energies extrapolation and transport codes such as MCNP [73] and GEANT-4 [46] are commonly used.

Backgrounds. Background suppression is possible with these detectors by identifying specific discrete γ rays that are characteristic of the product nucleus, a method that only works for known discrete γ rays and for full-energy deposition events.

To suppress the signal from events that were not full-energy deposition, "Compton shields" can be set up as anti-coincidence triggers. Higher intrinsic efficiency γ-ray detectors (such as BGO) placed around the detector system can detect γ rays that scatter from the HPGe detectors and provide a trigger to discard an event in the HPGe. γ rays from the product nucleus that are not known can be identified in coincidence with the full energy deposition of a known γ ray in another HPGe detector.

Coincidence triggers suppress energy- and sample-dependent backgrounds from other reactions occurring in the sample in a way analogous to the thresholds used in TAS measurements, and again bring in sensitivity to knowledge about the cascade. Measurements utilizing coincidence to a single or a few known discrete γ rays rely on the knowledge of what percent of all cascades emit those particular gammas, as well as whether any other reactions occurring at the same time emit γ rays with energies close enough to overlap in the HPGe signal. Scattered neutrons are a source of background in these measurements, but the signal of a neutron interacting with an HPGe detector is well-characterized and can be identified [74].

Flux determination and normalization. Fission chambers and monitor reactions can be used to measure the flux, ϕ, for both energy-differential and energy-averaged measurements, as explained in Section 2.1. The flux can be integrated over the runs to determine the fluence, Φ, retaining the neutron energy dependence if needed for energy-differential measurements in the HER.

Data analysis. The measured background-corrected γ-ray yields, $Y_\gamma(E_n)$, are used to determine the cross-section of the specific transition in the nucleus, as is done in reference [75],

$$\sigma_\gamma(E_n) = \frac{Y_\gamma(E_n)\tau_\gamma(1+\alpha_\gamma)\theta_\gamma}{\Phi(E_n)\tau_\phi\varepsilon(E_\gamma)d}. \tag{6}$$

In this equation, $\varepsilon(E_\gamma)$ is the γ-ray detector efficiency at the energy of the discrete γ ray and τ_γ is the dead time correction for the γ-ray detectors. The fluence, $\Phi(E_n)$, (in neutrons/MeV in this equation) is measured by a fission chamber and τ_ϕ is the dead time correction for that detector. θ_γ is the correction for the angular distribution of the emitted γ ray and $(1+\alpha_\gamma)$ is the correction for internal conversion of the transition, which allows for the determination of not only the γ-ray production cross-section, but the cross-section of the transition in the nucleus that emits the measured γ ray. The target thickness, d, is given here in atoms/mb. Different units can be used for many of these variables as long as they are self-consistent, and in some cases, a Beam Interception Factor correction, $\oslash$, may be needed.

The branching ratio or intensity of the specific transition is needed to determine the reaction cross-section. In decay sources the intensities of specific discrete γ rays are characteristic of the decay and can be taken from the evaluated structure database ENSDF [32]. The γ-ray cascade following a reaction is energy-dependent, and only relatively simple cascades at specific incident energies are fully known. Production cross sections of individual discrete γ rays are the most well-characterized for thermal neutron capture reactions [32,71] and are used in Prompt γ-ray Activation Analysis (PGAA) material identification measurements. Fully understood cascades can be used to determine the thermal capture cross section [76], but less well-known isotopes are often simulated with cascade generation codes [77–79]. Hauser-Feshbach codes [80–83] are used for HER measurements, where both the initial excitation and cascade need to be calculated. A detailed example of such a calculation can be found in reference [84].

2.2.4 Charged-particle detection

Facilities. In the case of charged-particle production reactions, the charged product can be measured directly at the time of the reaction. Gaseous detectors such as proportional counters [85], gridded ionization chambers [86–88] and compensated ionization chambers [89,90] can provide large solid-angle coverage and high intrinsic detection efficiencies. Solid state detectors such as silicon surface barrier detectors [4,91,92] and single crystal diamond detectors [93,94] allow for good energy and angle resolution and are less sensitive to γ rays. Scintillation detectors such as Li glass [95,96], ZnS [89], and CsI(Tl) [97] have fast timing resolution and high intrinsic detection efficiencies. Multiple detector types are often combined to take advantage of the differing strengths, such as the LENZ detector system at LANSCE [86] (Frisch grid ionization chambers and silicon strip detectors), the FAZIA collaboration [97] (silicon strip detectors and CsI(Tl) detectors), and the LPDA detector system at the CSNS Back-n facility [98] (silicon detector array and Frisch grid ionization chamber). A simple schematic of the measurement is shown in Figure 3d.

The stopping power of a charged particle in a detector is determined by the charge, Z, the mass, A, and the energy, E, which provides a mechanism for the identification of the particle. Detectors are often set up in a line, called a telescope configuration [99],

and the energy deposition in the detectors is used to determine the particle. The $\Delta E - E$ technique is used when a particle loses energy in one or more thin detectors and is fully stopped in a final, thicker detector. The energy loss (ΔE) in the thin detector, compared to the full energy of the particle (E) determined by the signal from the thicker detector, is used to identify the particle [99]. Particles that are not energetic enough to escape thin ΔE detectors can be identified using the Pulse Shape Analysis (PSA) technique [100,101], which uses characteristics of the signal in a single detector such as the rise time and the maximum of the current [97].

Sample characteristics. For direct charged-particle detection measurements, the sample should be as thin as possible to minimize energy loss by the emitted particles escaping the sample. If a sample is too thick, the reaction products could escape with too little energy to be detected or be stopped entirely in the sample.

Efficiency. The efficiency of these measurements is determined by the solid angle coverage, the intrinsic efficiency of the detectors, and the particle identification thresholds. The particle resolving power of a detector setup can be optimized for the type and energy range of the particles that will be measured. For a recent measurement of ^{59}Ni(n,p) and ^{59}Ni(n,α) with the LENZ detector [101], the silicon detector thicknesses were optimized to allow discrimination of protons and α particles down to $4\,\mathrm{MeV}$. Combined with the reaction Q-value, this allowed for the measurement of the ^{59}Ni$(n,p)^{59}$Co reaction up to outgoing proton energy of $(Q_p - 4\,\mathrm{MeV})$, and the ^{59}Ni$(n,\alpha)^{56}$Fe reaction up to an outgoing α energy of $(Q_\alpha - 7\,\mathrm{MeV})$. A calculation of the outgoing proton and α spectra was used to estimate the fraction of events below those thresholds.

Backgrounds. Common sources of background include signals from neutron and γ-ray interactions with the detectors, charged particles created by other reactions, and radioactive samples. Many of the detector systems require a lot of material near the sample (such as the vacuum chamber and detector housing) which the neutrons can interact with. Scattered neutrons can also interact directly with the detector materials, resulting in additional charged particles produced via reactions such as ^{28}Si(n,p), ^{28}Si(n,α), ^{12,13}C(n,p), and ^{12,13}C(n,α). These energy-dependent backgrounds can be measured and subtracted out [88,93], suppressed with data analysis thresholds [94,101], or characterized by Monte Carlo simulations using MCNP or GEANT and subtracted [102].

Background protons, such as knock-out protons from water-spray cooling of the neutron-production target, can be difficult to characterize with background measurements. The materials in the beam will degrade the proton energy, resulting in different measured proton spectra for the sample and background measurements. Reference [103] provides a detailed description of this effect and an example of the impact in proton-recoil measurements.

Flux determination and normalization. The flux for white neutron source measurements is often monitored using fission chambers or other neutron detectors, and the AP technique is often used for mono-energetic measurements. The flux can be integrated over the runs to determine the overall irradiation fluence.

Data analysis. The angle-differential cross-section is determined by,

$$\sigma_r(E_n, \theta) = \frac{(c - b)\tau}{\phi \; n \; \Omega_\theta \varepsilon \oslash}, \tag{7}$$

where c and b are the sample and background counts, respectively, ϕ is the flux, n is the number density of the sample, and ε is the efficiency. Corrections are made for dead-time losses, τ, the Beam Interception Factor, $\oslash$, and for the spread in θ due to the finite detector, Ω_θ. Multiple scattering corrections are typically negligible in these measurements due to the thin samples.

For many datasets, the yields are integrated over the outgoing energy and angle of the charged particles to determine the reaction cross-section. Legendre polynomials that fit the experimental data have historically been used for the angle integration, with assumptions on the underlying angular distributions made based on statistical reaction models [91]. Higher precision measurements and more sophisticated detector modeling has led to the need for improved angular distribution information, but current nuclear reaction evaluations often provide limited or no angular distributions for emitted charged particles [104]. To fill this gap, a new evaluation of proton and alpha energy- and angular distributions was performed for 62 isotopes, and validated with a LENZ measurement of a brass sample [104]. The study showed that the improved distributions led to qualitative and quantitative differences in the energy and angle distributions of the simulated proton and α yields, which produce differences in the calculated efficiency values used to integrate the observed yields over outgoing energy and angle. Similarly to the in-beam γ-ray detection methods, the charged-particle detection methods rely on either minimizing the sensitivity to the characteristics of the emitted particles (lower thresholds) or accurately modeling them (improved energy and angle distributions).

2.3 Specifics of offline reaction product measurements

Offline measurements separate the irradiation of the sample and the detection of the reaction, avoiding the complex time-dependent backgrounds of in-beam measurements. The most common method is by Activation Analysis which can be used when the product nucleus is radioactive and the reaction yield is determined by observation of the decay. Mass Spectrometry can be used to directly count the number of product nuclei in the sample if the cross section is too low or the product does not have a suitable half-life. Schematics of the measurement types are shown in Figure 4.
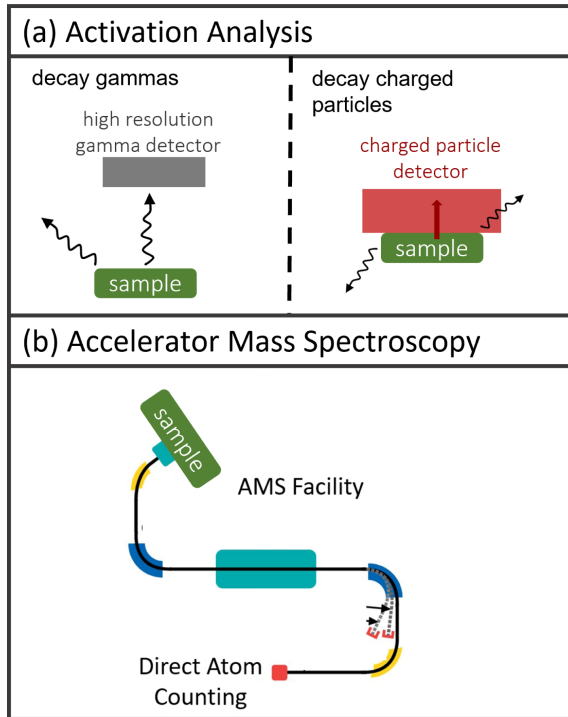
Fig. 4. Schematics for offline measurement types: (a) shows activation analysis measuring either decay γ rays or decay charged particles. (b) Shows Accelerator Mass Spectroscopy.

2.3.1 Activation analysis

Facilities. Activation Analysis (AA) is a common measurement technique when the product is radioactive with a half-life between seconds and weeks. The sample is irradiated by a neutron source and then moved to a separate low-background counting location. A schematic of an AA measurement is shown in Figure 4a.

Decay γ rays are typically measured with high-resolution HPGe or Ge(Li) detectors to allow for the identification of discrete characteristic γ rays. Charged particles are often measured with silicon detectors such as Passivated Implanted Planar Silicon (PIPS) [105–108]. A detailed presentation of the data analysis equations and uncertainties for AA measurements utilizing decay γ rays is given in reference [109].

Sample characteristics. Samples are typically thin to avoid multiple scattering and attenuation of the measured decay products. When charged-particle products are measured, this is an especially important concern. If a monitor reaction is used for the flux normalization, any differences in the geometry of the two samples should be corrected for.

Efficiency. Calibration sources can be used to determine the intrinsic efficiency of γ-ray detectors, with simulations or curve-fitting used for interpolation and extrapolation to γ-ray energies not measured. The setup for an AA measurement often includes a single HPGe or Ge(Li) detector

close to the sample, with a large solid angle to counteract the low intrinsic efficiency. The higher count rate improves statistical uncertainties, but at the risk of introducing coincidence summing effects. True coincidence summing occurs when multiple γ rays from a single decay event interact with the detector simultaneously. The magnitude and impact of coincidence summing depends on the distance between the sample and detector, count rate, and γ-ray cascade being measured, and can only be accurately simulated and corrected if the cascade is well-modeled. For decay sources with simple cascades this can be done analytically [110], and Monte Carlo methods have been developed for more complex decay schemes [111]. For cascades that are not well-known, the calibration source or sample should be moved far enough away from the detector to avoid coincidence summing effects, which can be validated by comparing the spectra at different distances, as was done with calibration sources in reference [112].

The efficiency of charged-particle detectors can be determined by simulations that account for the solid angle subtended by the detector and model the energy loss of the particles [106,107]. Validation can be done using well-characterized α or β decay sources [107], and sources with spectra similar to the sample should be used when possible.

Backgrounds. Backgrounds in AA measurements are typically easier to minimize and characterize than the time-dependent beam backgrounds. The counting location should have a well-characterized room background that is routinely measured to low statistical uncertainties. Sample-dependent backgrounds include charged particles or γ rays emitted from other decay processes in the sample and Compton scatters for γ-ray measurements. The behavior of the signal over time can help to determine if there is a background from another decay process, as it should follow the half-life of the decay.

Flux determination and normalization. For offline measurements the measured reaction yield, Y, is a function of the true cross-section integrated over the irradiation time, t, the beam energies, E_n, and the solid angle, Ω,

$$Y = \int dt \int dE_n \ \sigma(E_n) \ \times$$
$$\int d\Omega \ \phi(E_n, r, \theta, \varphi, t)\rho(r, \theta, \varphi), \tag{8}$$

where $\sigma(E_n)$ is the true reaction cross-section at incident energy E_n, ρ is the areal density of the sample, and ϕ is the flux, given in cylindrical coordinates (r, θ, φ). In the case of a strongly fluctuating neutron beam a correction term, $\Delta\phi$, should be used,

$$Y = t\Delta\phi \int dE_n \ \sigma(E_n) \int d\Omega \ \phi(E_n, r, \theta, \varphi)\rho(r, \theta, \varphi). \tag{9}$$

The integral over the Beam Interception cross-sectional area reduces to the mass of the sample, M, for an overfilled sample, Figure 1a,

$$Y_o = t\Delta\phi \ M \int dE_n \ \sigma(E_n) \int d\Omega \ \phi(E_n, r, \theta, \varphi) \tag{10}$$

but the yield depends on the spatial distribution of the beam. The sample areal density is important for an under-filled sample, Figure 1b, and the integral of ϕ over the Beam Interception area reduces to the current of neutrons, I,

$$Y_u = t\Delta\phi \int dE_n \ I(E_n)\sigma(E_n) \int d\Omega \ \rho(r,\theta,\varphi). \quad (11)$$

These equations show how the measured yield can be modeled as a function of the true cross-section, the sample, and the flux. In practice, most data analysis is not performed by forward modeling using these relationships, instead using the fluence, Φ, which is the time-integrated flux. A correction factor for beam fluctuations, $\Delta\phi$, can be used explicitly or included in the fluence calculation. Alternatively, the quantification of Φ can be avoided by the use of a monitor reaction, as explained in Section 2.1.

Data analysis. The measured counts give the activity at the end of the irradiation, A_0, which is used to determine the reaction cross-section, σ_r, in a similar manner to γ-ray spectroscopy, equation (6),

$$\sigma_r = \frac{A_0\tau\oslash}{n\Phi I_\gamma f\varepsilon}, \quad (12)$$

where n is the number density of the sample. The detection efficiency for the measured γ ray or charged particle is ε, and τ is the dead time correction for that measurement. I_γ, the intensity for the specific γ ray or charged particle measured, is often given as a number of emissions per 100 decays in the evaluated structure library ENSDF [32].

The time factor, f, is used to account for simultaneous production and decay during the irradiation time, t_i, decay during the cooling or waiting time, t_w, and the measured decay during the counting time, t_c,

$$f = \frac{1}{\lambda} \left(1 - \exp^{-\lambda t_i}\right) \exp^{-\lambda t_w} \left(-\exp^{-\lambda t_c}\right), \quad (13)$$

where λ is the decay constant for the specific decay measured for the sample [109].

The fluence, Φ, can be measured directly and included in equation (12), with corrections for the Beam Interception Factor, $\oslash$, and beam fluctuation, $\Delta\phi$, made when appropriate. If a monitor reaction is used to determine the fluence, the equation simplifies to a ratio of quantities for the sample, s, and the monitor, m,

$$\sigma_r = \sigma_m \frac{A_s\tau_s\oslash_s}{A_m\tau_m\oslash_m} \frac{n_m I_m f_m \varepsilon_m}{n_s I_s f_s \varepsilon_s}, \quad (14)$$

where σ_m is the cross-section of the monitor reaction. The use of a monitor allows for many quantities to be simplified. For example, the absolute efficiencies ε_s and ε_m do not need to be quantified, only the ratio $(\varepsilon_s/\varepsilon_m)$.

2.3.2 Mass spectrometry

For measurements where acceptable statistical uncertainties cannot be attained with activation analysis because of a small cross-section or a long half-life, the sample can be destructively analyzed to directly estimate the number of product nuclei produced. Direct counting can also be used to count reaction products that are not radioactive, as has been done to count the α particles created by (n,α) reactions on many materials using gas mass spectroscopy [1,113]. Accelerator Mass Spectroscopy (AMS) extends the mass spectrometry method with the ability to separate ions by nuclear charge as well as mass [114], allowing for the identification of specific isotopes. The AMS method can quantify ratios of isotopes down to 10^{-16} in ideal cases [5] which allows for the detection of low-yield reaction products such as $^{54}Fe(n,\gamma)^{55}Fe$ against the large background of other iron isotopes [115]. Atom trap trace analysis [116] has also been used to directly count noble gas product nuclei [117]. AMS is the most commonly used of these methods for cross-section measurements, and is the only mass spectrometry method discussed in detail in this work.

Facilities. AMS has become a popular method to measure reactions of astrophysical importance such as $^{54}Fe(n,\gamma)$ [115], $^{62}Ni(n,\gamma)$ [118], and $^{40}Ca(n,\gamma)$ [119], at facilities such as the Vienna Environmental Research Accelerator (VERA) [120,121], the Argonne Tandem Linac Accelerator System (ATLAS) [122,123], the University of Tokyo [124], and at the Maier-Leibnitz Laboratory [125,126]. The result of AMS measurements is the ratio of the rare isotope to a more abundant isotope (sometimes called the stable isotope), and for cross-section measurements, this is often the ratio of the product nucleus to the target nucleus.

All-atom counting methods are destructive, with atoms vaporized from a melted sample for gas mass spectrometry [1], sputtered from the surface of a solid sample for AMS [114], or laser trapped from gas samples for atom trap analysis [117]. In the case of AMS measurements, the sputtered atoms are passed through a carbon foil or gas to strip off electrons, leaving individual charged ions. The trajectory of the ions is based on their charge state and mass, so accelerated ions will naturally spread apart over a distance. Mass and charge resolution can be optimized with the flight path, charge state, and resolving magnets. TOF can be used for even higher resolution but is typically only needed for high-mass isotopes [127].

The more abundant or stable isotope can be measured as a current in a Faraday cup detector, while the atoms of the rare isotope are usually measured individually with particle detectors such as ionization chambers or silicon detectors. More details on AMS measurements can be found in references [127–129].

Sample characteristics. The sample size and geometry are not an important concern for AMS measurements, as the method is destructive and directly counts atoms. In many cases, a sample weighing just a few milligrams can provide sufficient statistics, and the main concern is that the sample is a chemical form suitable for sputtering negative ions [5].

Efficiency. The efficiency of AMS measurements varies widely, as it depends on the detectors used, the extraction efficiency for the particular negative ions, and the transmission of the ions through the system. Typical values are on the order of 10^{-5} to 10^{-2} [5]. Quantification of the absolute efficiency can be avoided with the use of a standard calibration sample that has well-characterized isotope ratios, which is commonly done. Such standard samples can be difficult to create for the rare isotopes that AMS is often used for. Reference [130] describes the process to create standard samples for measurements of ^{55}Fe, ^{68}Ge, and ^{202g}Pb, where the knowledge of the isotopic composition of the ^{55}Fe standard was limited by the uncertainty in the half-life of ^{55}Fe. When such a standard is not available, the differences in efficiency between the rare and stable isotopes must be determined for the transmission, the charge state yields, and the intrinsic detector efficiencies. An example of a measurement without a standard is given in reference [131].

Backgrounds. One background source unique to AMS measurements is from isobars and isotopes whose trajectories also lead to the detectors. The suppression of this sample- and energy-dependent background is specific to the measurement, such as choosing a very high charge state (15^+) in a ^{79}Se measurement to reduce the signal from ^{79}Br [126], or a negative charge state to reduce the background signal from ^{26}Mg in a measurement of ^{26}Al [132]. In many cases, the charge state chosen to minimize background is not one that would be chosen to maximize efficiency.

Atoms of the product nucleus present in the sample before the irradiation are also a source of sample-dependent background for AMS measurements to determine cross sections. "Blank" samples that have not been irradiated can be measured to quantify the initial presence of the product nucleus in the sample, and the cross-section can be determined based on the difference in the product-to-target ratio in the two samples. This background subtraction is usually implicit in the data analysis equations.

Flux determination and normalization. The fluence is often measured using monitor reactions chosen based on the spectrum used for the measurement. The monitor sample is not usually destructively analyzed by AMS, so the simplification to ratios often used in AA, equation (14), is not possible.

Data analysis. As the result of an AMS measurement is the ratio of the number of atoms of the product, n_p, to the number of atoms of the target, n_t, in the irradiated sample, $\frac{n_p(E_n)}{n_t(E_n)}$, the reaction rate equation can be simplified,

$$\sigma_\gamma(E_n) = \frac{1}{\Phi(E_n)} \frac{n_p(E_n)}{n_t(E_n)}, \tag{15}$$

where corrections for background have already been applied. The fluence can be determined by direct measurement or in ratio to a monitor reaction.

3 Information needed for evaluations

3.1 Evaluation methodologies

In the RRR, evaluated cross sections are represented with R-Matrix theory [133] using parameters of individual resonances, and in the URR using averaged parameters. The RRR parameters are evaluated with dedicated codes such as SAMMY [134], REFIT [135], and EDA [136], which make use of chi-squared-based minimization or Bayesian updating. Reaction cross sections are proportional to the product of the neutron width, Γ_n, and the reaction width, Γ_r,

$$\sigma_r \propto \Gamma_n \Gamma_r, \tag{16}$$

for each resonance.

EDA is used for evaluating light nuclei with the full multi-channel, relativistic R-Matrix formalism needed to properly represent the various scattering, capture, and charged-particle production channels that can be experimentally characterized [137]. For nuclei heavier than $A \sim 20$, charged-particle production reactions are rarely open in the RRR, and the Reich-Moore approximation [138] is commonly used for capture in SAMMY and REFIT. The Reich-Moore approximation assumes that there are enough γ-ray transitions out of the capture state to represent the distribution of Γ_γ as a chi-squared distribution with a large number of degrees of freedom, which asymptotically goes to a chi-squared distribution with infinite degrees of freedom,

$$\Gamma_\gamma \sim \chi_\infty, \tag{17}$$

which is a delta function around the average, $\bar{\Gamma}_\gamma$.

The experimental observable in the RRR is reaction yield, an integral quantity affected by all resonances with the same spin and the experimental characteristics. An R-Matrix analysis is used to calculate a zero-temperature, theoretical cross-section from the resonance parameters which is then Doppler-broadened and convoluted with the experimental resolution function to obtain a quantity that can be directly compared with the experimental yield.

In the URR the evaluated cross-section is represented by averaged resonance parameters, and measurement results can be provided as yield or cross-section if the correction factor F_γ, equation (2), has already been applied.

In the HER, the cross-section is modeled as a smooth function of incident neutron energy, and Hauser-Feshbach (HF) theory [139] is used to describe reaction cross sections by transmission coefficients that sum to the total cross-section. HER evaluation codes such as EMPIRE [81], CoH [82], and TALYS [83] use various structure and reaction theories to calculate total and reaction cross sections. The models and parameter values that produce cross sections that best match the available experimental cross-section data are used to create point-wise evaluations of cross-sections and outgoing particle distributions.

3.2 Reporting systems (RRR-URR)

The Analysis of the Geel Spectra (AGS) framework [140, 141] can be used to report RRR capture yield and URR average capture cross sections. The AGS format allows for a simple reconstruction of the covariance matrix by providing the values and sensitivities of correlated and uncorrelated uncertainty sources. The background function, equation (1), is represented as the product,

$$\dot{B}(t) = K\dot{b}(t), \tag{18}$$

where K represents all terms with sources of correlated uncertainty and $\dot{b}(t)$ involves all terms with uncorrelated uncertainty sources. This allows evaluators to understand and modify the final uncertainties on these datasets if needed.

In the RRR, experimental metadata is required due to the forward modeling of the yield. Discussions of what information should be provided to EXFOR [142] were held at the IAEA Consultant's Meeting on EXFOR Data in the Resonance Region and Spectrometer's Response Functions. A summary of the meeting and recommendations are documented in reference [143], along with a template for experimental metadata. Metadata and resolution functions are provided for several EXFOR entries on the meeting web page.

As the EXFOR entry is often the main (and sometimes only) source of information about an experimental dataset used by evaluators, the entry should include as much of this metadata as is necessary to model or check the dataset. Information that is not reasonable to compile, such as long descriptions of simulations or corrections, is usually referenced in the entry.

3.3 Experiment metadata

The minimum information needed for an evaluator to use a dataset is the values and total uncertainties of the measured observable (the reaction yield or cross-section) and of the incident neutron energy values or spectrum. It should be made clear what the observable is, and in the compilation of the dataset, the yield data should not be converted to the units of cross-section by dividing out the sample thickness, even when the thin-sample approximation is valid.

As detailed in reference [143], RRR datasets should come with enough information to accurately model the experimental setup in the evaluation process. This includes the sample dimensions, composition, and temperature. The neutron source and detector setup are modeled in the resolution function, $R(t_t, E_n)$, which is needed by evaluators to compare the theoretical cross-section to the measured reaction yield data. Resolution functions can be provided in terms of functional forms, in tabular form, or as inputs to the commonly-used RRR codes.

Facilities. The neutron source should be described in detail. For RRR measurements with TOF, the neces-

sary information is usually included in the resolution function.

The flight path and repetition rate can be helpful for determining the energy resolution and possible overlap, or "wrap-around" of low-energy neutrons from the previous pulse. However, a detailed understanding of the facility is needed to determine such effects and it is not something a data user should be expected to calculate. The effects of wrap-around on the particular dataset should be provided with a discussion of the neutron source and background sources.

Filters can be placed in the beam to reduce overlap, minimize and/or quantify the background, and calibrate the neutron energy. Any filters used should be reported with each dataset to allow users of the data to understand structures not attributable to the sample being measured, which may render the dataset unusable in certain energy regions.

The neutron energy resolution is important for characterizing the measurement observable. The time bin widths and edges in TOF experiments and the neutron energy distribution in mono-energetic experiments allow users of the data to understand the ability of the measurement to detect underlying fluctuations in the cross sections, and to verify the resolution if needed.

If the beam non-uniformity was assessed, a description can be useful for comparisons of datasets between facilities–even if the non-uniformity was determined to not require a correction.

The detectors used and the general setup should be reported. In the case of a large detector array frequently used for measurements, a reference to previous work documenting the system is often provided. This should be accompanied by details of the detector setup that can change between measurements (such as the number of individual detectors, the voltages, or coincidence triggers).

Sample characteristics. The sample geometry and composition should be provided along with the uncertainties on these values. Corrections made (or determined to be negligible) should be described, including multiple scattering, attenuation in the sample, Beam Interception Factor, and sample non-uniformity. For RRR measurements some of this information is included in the resolution function, but additional information such as the sample temperature is needed as well.

Efficiency. The methods and standards used for efficiency calibration should be documented, especially in the case of extrapolation or simulation, along with their estimated uncertainties. If the efficiency simulations require γ-ray cascade calculations, the code and input values used (and ideally a plot of the produced spectrum) should be detailed along with any thresholds or cuts used in data analysis. This information would allow for the efficiency values and/or uncertainties to be reassessed in the future if more accurate cascade simulations become available. Descriptions should be provided for any corrections made for dead time, coincidence summing, or counting geometry/solid-angle coverage, along with the uncertainties for the corrections.

Backgrounds. The background characterization, suppression, and/or subtraction methods should be detailed for all sources of background in the experiment. Background sources determined to be negligible should be reported as such. Values and uncertainties for each data point should be provided when reasonable, as is done in the AGS system [140,141] with equation (18).

For background suppression techniques such as thresholds, coincidence triggers, and high charge states, estimates of the impact on the efficiency can help the users of the datasets to understand the background and efficiency uncertainties. Background suppression methods are typically tested and/or validated in the course of the experiment, but the valuable results and insights are not always included in the final documentation.

For backgrounds that were subtracted out, any nuclear data used for the calculation should be reported in enough detail to allow for future assessment if needed.

Flux determination and normalization. The method of flux determination or normalization should be described. If the flux is measured directly, the same information about the detectors and backgrounds should be provided as for the sample measurement. If monitor reactions were used, the sample, detector, and background information should be provided for this measurement.

For anything quantified only in the ratio (for example, the γ-ray detector efficiency at two energies) the method of calculating that ratio and the uncertainty on it should be documented. This is especially important in TAS and TED measurements when a saturated resonance in another isotope is used for normalization and the ratio of the overall system efficiency for the two isotopes is based on complex cascade and transport simulations, and based on isotope efficiency ratios such as the terms F_1 and F_2 in equation (2).

Data analysis. Providing the basic equations used in the data analysis process allows an evaluator to understand the sensitivities of various uncertainty sources. Although many uncertainty sources are multiplicative factors in the equations, some important uncertainty sources such as backgrounds and times have more complicated dependencies. If the experimental data analysis involved forward modeling or simulation, a description of the simulation process and an estimate of the uncertainties are important. Even when the forward-modeling process is described in a cited reference, a review of the process and any deviations from the previous work is very helpful for a user of the data.

If the experiment involved any characteristic time periods relevant to the data analysis, such as the irradiation, waiting, and counting times in AA measurements, their values and uncertainties are important for understanding correlations in the dataset. Even if the time uncertainties are determined to be negligible, the values themselves are useful.

For URR datasets that have been converted from capture yield to cross-section, the correction factor F_γ should be provided along with a detailed description of how the correction was calculated. Ideally, these mea-

surements would be provided with the uncorrected yield values as well. The self-shielding correction relies on the cross-section and can be performed iteratively and self-consistently by the evaluator.

For all reference data, the source of the values and/or the values themselves should be recorded so that updated values can be used in the future.

For reference data that are not taken from evaluated libraries such as ENSDF or ENDF, more information should be provided to allow for a full understanding of the uncertainties. Calculations of outgoing particle energy- and angle-distributions and γ-ray cascades should be documented in detail as future use of the dataset may require a reassessment of the reference values or uncertainties.

4 Template

If a dataset does not provide complete uncertainties, the evaluator needs to estimate some values in order to do a fair comparison with other datasets. When possible, missing information should be obtained specifically for that dataset by reviewing other reports or articles about the facility, detector system, sample, etc. This template serves as a source of reasonable uncertainty estimates in cases where specific information cannot be obtained. The uncertainty templates for the in-beam resonance region measurement types TAS and TED are provided in Table 1 and for the other methods in Table 2.

These templates also provide recommendations for correlations within and between experiments, which evaluators need to estimate more often than the uncertainties. Correlations are described by a shape, which defines the energy dependence, and a magnitude. The two shapes used in this work are constant in energy and a "Gaussian" dependence in energy, where a Gaussian is used to represent a correlation that is stronger between data points closer in energy. Reference [144] gives the following equation,

$$\text{corr}(i,j) \propto \exp\left[-\left(\frac{E_i - E_j}{\max\left(E_i, E_j\right)}\right)^2\right], \qquad (19)$$

where E_i and E_j are the incident neutron energies of points i and j.

4.1 Facilities

4.1.1 Neutron energy ($\delta E_n, \Delta E_n$)

For TOF measurements, the energy uncertainty, δE_n, and/or resolution, ΔE_n, are difficult to estimate as they depend on the flight path, the timing resolution of the detectors, and the neutron energy itself. In RRR measurements this uncertainty is usually provided in the resolution function. If estimation is needed, it should be based on experiments at the same facility.

For spectrum-averaged thermal or MACS measurements, the neutron energy uncertainty is typically

Table 1. Uncertainty template for in-beam resonance region measurement types TAS (2.2.1) and TED (2.2.2). The values given are relative uncertainties in percent. Parameters with no recommended uncertainty values are left blank. The correlations provided here are between different data points within the same experiment. The variables are defined in the following sections.

	Uncertainty source		TAS, TED (%)	corr(i, j)
(4.1.1)	ΔE			Strong Gaussian
(4.2.1)	δn		see Table 3	Fully
(4.2.2)	δw		see Table 3	Fully
(4.2.5)	$\delta \dot{c}$			Uncorrelated
(4.3.1)	$\delta \dot{b}$			Uncorrelated
(4.3.2)	δK		3	Fully
(4.3.2)	$\delta \dot{B}(t)$		3	Strong Gaussian
(4.4.3)	δN_γ	(internal res.)	1–2	Fully
		(external res.)	2–6	
(4.4.4)	δF_γ			Fully

Table 2. Uncertainty template for in-beam measurement types γ-ray spectroscopy (2.2.3) and direct charged-particle detection (2.2.4) and offline measurement types AA (2.3.1) and AMS (2.3.2). The variables are defined in the following sections. The values are relative uncertainties, given in percent, on the parameter. Parameters with no recommended uncertainty values are left blank, and those that are not applicable to the measurement method are denoted with a hyphen, "–". The correlations provided here are between different data points within the same experiment.

	Uncertainty source		γ-spec (%)	CP (%)	AA (%)	AMS (%)	corr(i, j)
(4.1.1)	δE		1	1	1	1	Strong Gaussian
(4.2.1)	δn		Table 3	Table 3	Table 3	–	Fully
(4.2.2)	δw		Table 3	Table 3	Table 3	–	Fully
(4.2.3)	δm		Table 3	1–2	Table 3	–	Strong Gaussian
(4.2.5)	δc						Uncorrelated
(4.2.6)	$\delta \varepsilon$	(γ-ray)	Table 4	–	Table 4	–	Fully
		(CP)	–	2–5	2–5	–	Strong Gaussian
(4.2.8)	$\delta \Omega_\theta$			1			Fully
(4.3.3)	δb	(AMS)	–	–	–	5	Uncorrelated
(4.4.1)	$\delta \Phi$	(monitor)	–	–	2–5	2–5	Strong Gaussian
		(AP)	–	–	1–3	1–3	
(4.4.2)	$\delta \phi$	(direct)	≥ 3	≥ 3	–	–	Strong Gaussian

expressed as part of the "thermal equivalent" flux uncertainty.

For mono-energetic neutron sources, the uncertainty depends on the reaction used, but 1% is a reasonable uncertainty for most reactions, as given in Table 2. For smooth cross sections this uncertainty can reasonably be neglected as inconsequential to the use of the dataset.

Between data points in the same experiment and between experiments at the same facility and flight station, the uncertainties are likely to have a strong Gaussian correlation as given in Tables 1 and 2. Experiments with the same source but different flight paths are likely to have a moderate Gaussian correlation, and a weak correlation is expected between experiments with different neutron

sources at the same facility, as the methods of characterizing the energy are likely to be similar.

4.1.2 Resolution function $(\delta R(t_t, E_n))$

The resolution function is used to model RRR datasets in the evaluation process, so the uncertainty, $\delta R(t_t, E_n)$, is needed for proper uncertainty propagation through the evaluation process. Uncertainties on the parameters are not often provided in publications, and when they are provided it is not always clear how they could be used in the current RRR evaluation codes. For example, the RRR code SAMMY has functional forms with default values that can be used for the RPI, ORELA, GELINA, and n_TOF facilities, but the various parameters cannot

Table 3. Uncertainty template for sample characteristics number density, δn, composition, δw, and multiple-scattering correction, δm. The values are relative uncertainties, given in percent, on the parameter.

	Uncertainty source		Value (%)
(4.2.1)	δn	(metal)	0.1–1
		(powder)	2–5
		(liquid)	0.1–1
		(diluted liquid)	2–5
(4.2.2)	δw	(stable)	0.1–1
		(radioactive)	1–3
(4.2.3)	δm	(thin)	0.5–2
		(thick, well-known)	2–5
		(thick, not well-known)	5–20

always be clearly connected to the information provided in a publication or EXFOR entry. The template created by the IAEA Consultants' meeting on EXFOR resonance region data [143] includes important metadata about the experimental setup, but does not generally provide these specific parameter values and uncertainties. One recommendation from this meeting was to create a database of resolution function values for EXFOR entries, and the specific values needed in the evaluation are available for several datasets [145–148]. For a few datasets, the exact lines to use in the SAMMY input file are provided, which includes the uncertainties on the parameters, but for others, only parameter values are given. More work in this area is needed before recommendations on how to estimate resolution function forms, parameters, and/or uncertainties can be given.

4.2 Sample characteristics

4.2.1 Target number/areal density (δn)

The number density of the sample, n, is used to determine various quantities in the analysis equations, including as the sample thickness, the areal density, or the mass. The uncertainty, δn, depends on the physical form of the sample, which is detailed in Table 3. Metal samples are the easiest to characterize and can have uncertainties between 0.1% and 1% unless the sample thickness measurement is difficult. Powder samples are more difficult to characterize due to air pockets and water absorption, and an uncertainty between 2% and 5% is more common. Naturally liquid samples are expected to have uncertainties on par with metal samples, but liquid samples created by dissolving a solid sample have larger uncertainties and 2%–5% is reasonable. Diluted liquid samples are created by dissolving a sample in order to lower the effective n and improve measurements of very high capture cross sections in the resonance region [149].

For most measurements, a single sample is used at all presented neutron energies, in which case the uncertainty δn is fully correlated for all data points. For some HER measurements, different samples are irradiated with different neutron energies. The δn correlations between data points in this case depend on the sample creation and characterization methods–if they are the same for all samples, a strong, constant correlation is expected. Between experiments, δn correlations can be hard to determine. Commercially-produced samples are typically characterized at the experimental facility, so a moderate correlation is expected for experiments at the same facility. This is also true for samples created in-house, as they are likely to be characterized with the same equipment and methods. Samples of rare isotopes are often exchanged between facilities and used for many experiments, but such samples should be characterized at each facility and before each experiment. At facilities that use the same methods for characterization, weak correlations are expected.

4.2.2 Sample composition (δw)

The uncertainty on the sample composition, δw, is dependent on how common the isotope is and whether it is stable. For natural abundance samples, literature values should be used[2]. A sample enriched in a relatively common isotope that is stable can have δw as low as 0.1–0.3%, but this is difficult to achieve, and without further information, an estimate of 1% is reasonable, as given in Table 3. A sample enriched in a common radioactive isotope is likely to have a higher uncertainty which is dependent on the characterization method. δw between 1% and 2% is reasonable, but if no information is provided an estimate of 3% is recommended. Samples enriched in rare isotopes, whether stable or radioactive, are hard to estimate generally. The δw correlations are similar to the δn correlations, as they are based on characterization methods.

4.2.3 Multiple-scattering and attenuation corrections (δm)

How multiple scattering was addressed should be explained in detail, as this correction can vary widely between experiments. The recommended values are given in Table 3.

For very thin samples, as are usually used for in-beam direct charged-particle measurements and AMS measurements, multiple scattering is likely to be negligible but attenuation of the outgoing charged particles may not be, so an uncertainty of 1%–2% is reasonable if there is no information about such a correction.

Multiple scattering corrections are typically done with analytical calculations or simulations that rely on the cross-sections of the isotope being measured. The correction becomes more important with increasing sample thickness as the average number of scatters increases and errors in the correction compound. For thin samples, if the correction was not determined to be negligible, δm

---

2 If the natural abundance of the element varies by location, the literature uncertainty should be increased to account for the known variation.

values between 0.5% and 2% are reported. If this uncertainty needs to be estimated, the evaluator should consider how well the scattering cross sections were known at the time of the experiment and the average number of scatters expected with the current nuclear data to decide if the value should be at the lower end or higher end of this range.

For thick samples the average number of scatters and the magnitude of the correction are likely to be much higher, so the quality of the scattering cross sections used in the correction becomes more important. For corrections performed with nuclear data that were well-known at the time of the experiment, a conservative estimate between 2% and 5% is reasonable if there is no specific information. For corrections performed with nuclear data that were not well-known at the time, a larger uncertainty should be assumed, upwards of 5%. If simple methods were used to calculate the correction (such as first-order approximations in analytical calculations), an uncertainty of up to 20% may be warranted.

The energy dependence of the multiple scattering corrections is based on the cross sections, so with smooth cross sections the correction is likely to be relatively constant across energy points. However, in most cases the cross sections vary with energy, and a strong Gaussian correlation is recommended in the absence of any specific information. Between experiments, the underlying nuclear data is the strongest driver of the correlation on δm, unless very simple approximations dominate the uncertainty. If the same approximate methods and/or nuclear data were used, a strong correlation is recommended.

γ-ray attenuation corrections in TAS and TED measurements are accounted for in the overall system efficiency normalization. In γ-spectroscopy and AA measurements, γ-ray attenuation coefficients are used when attenuation is significant. These coefficients are based on photon transport models which allow for negligible uncertainties in the absence of complicated or poorly-modeled geometry, so no recommended values or correlations are provided.

4.2.4 Beam interception factor ($\delta\oslash$)

The uncertainty on the Beam Interception Factor correction, $\delta\oslash$, is negligible in most experiments and difficult to generalize when it is significant. No recommended uncertainties or correlations are provided, but detailed explanations of the Beam Interception Factor correction in references [21,150] may be a useful guide for making an estimate.

If a correction was made, the uncertainty will be fully correlated between data points using the same sample, and strong correlations are expected between experiments at the same facilities using the same methods.
Efficiency.

4.2.5 Counting statistics ($\delta c, \delta\dot{c}$)

The uncertainty on the counts, δc, and count rates, $\delta\dot{c}$, cannot be estimated, so no recommended values are provided in this template. Datasets that do not report even

Table 4. Uncertainty template for γ-ray detector efficiencies. The values are relative uncertainties, given in percent, on the parameter.

E_γ [MeV]	$\delta\varepsilon$ (%)
<0.2	4
0.2–2.6	2
>2.6	5

the counting statistics should be used with caution. For RRR measurements, counting statistics can be a dominant source of uncertainty between resonances but a minor source of resonance peaks. Counting statistics are uncorrelated between data points and between experiments.

4.2.6 Efficiency ($\delta\varepsilon$)

The uncertainty on the detector efficiency varies widely between detector types. For γ-ray detectors, the uncertainty is the lowest for γ rays between 0.2–2.6 MeV, where there are widely available calibration sources, as seen in Table 4. In this region, uncertainty values between 1% and 3% are commonly reported, and an estimate of 2% is recommended when there is no additional information. Below 200 keV and above 2.6 MeV, calibration sources are not common and the uncertainties recommended are higher, 4% and 5%, due to the need for extrapolation. If a specific calibration source in those regions was obtained or created for a particular experiment and the method is well-documented, the lower value of 2% is reasonable. Below 200 keV the efficiency of HPGe turns over (begins to decrease), and a specific calibration source used to constrain the shape is needed for 2% to be reasonable. If coincidence summing corrections are needed, the efficiency uncertainty will be higher, but the difference is hard to generalize. A method for propagating coincidence summing uncertainties is presented in reference [151] which users of the datasets are encouraged to follow if an estimate is needed.

For charged-particle detectors, the reported uncertainties range between 0.5% and 5%, depending on the sophistication of the simulations to correct for the lower-level discriminator, and on how the calibration was performed. If the uncertainty is not provided and must be estimated, a conservative value between 2% and 5% is recommended.

The efficiency uncertainties for TAS and TED measurements are included in the normalization simulations and are not presented separately.

Efficiency uncertainties are fully correlated between data points within an experiment when the same particle energy is measured for each data point, as is done in γ-spec and AA measurements. For direct charged-particle measurements, a strong Gaussian correlation is expected due to the dependence of the outgoing particle energy on the incident energy. Between experiments a weak Gaussian correlation is expected if the same calibration methods and/or calibration sources were used; otherwise, no correlation is expected.

4.2.7 AMS relative efficiency

In AMS measurements, a standard sample can be used to determine the relative efficiency for detecting the target and product nuclei. The efficiency uncertainty with standards varies widely based on the standard–in one study that focused on the creation of standards, an uncertainty of 1.6% is reported for a ^{55}Fe standard created from a reference solution, and between 5% and 7% for a ^{202}Tl standard [130].

Without such a standard, the uncertainty on the relative efficiency is unlikely to be less than 5%–10% [152]. An absolute measurement of the ^{209}Bi$(n,\gamma)^{210m}$Bi [125] cross-section used beam-attenuation to quantify the ratio and quoted an uncertainty of 5%, the low end of the expected uncertainty range.

The uncertainty due to the relative efficiency is usually documented for AMS measurements due to the wide variation and typically significant magnitude. For this reason, no recommended values or correlations are provided.

4.2.8 Solid-angle correction ($\delta\Omega_\theta$)

Angle-differential cross-sections are reported at specific angles, but the detectors used are finite in size. The correction for the solid-angle subtended by the detectors, Ω_θ, is generally reported with small uncertainties, between 0.3% and 1% in the literature [153,154]. If no uncertainty is given for this correction, the upper end of the range, 1%, is recommended in Table 2 as a conservative estimate. This uncertainty is fully correlated between data points in an experiment but no correlations are assumed between experiments.

4.2.9 Counting geometry correction

If the efficiency calibration of a high-resolution γ-ray detector was performed using calibration sources of significantly different sizes or shapes from the sample, a counting geometry correction may be needed. The uncertainty on this correction is typically included in the efficiency uncertainty, so no specific geometry correction uncertainties or correlations are recommended.

4.2.10 Dead time correction ($\delta\tau$)

Corrections for dead-time losses in detectors have negligible uncertainties in many modern experiments, which purposefully minimize the dead-time correction magnitudes. Measurements with thick samples [155] or with high γ-ray rates [75], however, still have significant dead time corrections. Dead time corrections are often applied to the count rates before the counting statistics uncertainties are determined. For this reason, if no dead time uncertainties are provided but it is suspected that they would be significant, it is recommended that the counting statistics uncertainties are increased by an appropriate amount. Just as with the counting statistics, this uncertainty is difficult to estimate for an experiment both in magnitude and sensitivity. For example, a study of dead time correction effects with a thick Au sample showed that for one resonance, a change in the dead time correction magnitude by a factor of 2.2 had only a 2% effect on the yield [155].

No recommended values or correlations are provided for $\delta\tau$, as this uncertainty is often included in the counting statistics or is negligible. The correction can be energy-dependent and can induce correlations between neutron energy bins in TOF measurements, which is accounted for in the AGS analysis software [140]. Reference [156] provides equations that can be used to estimate the correlation if enough information is provided and it is not clear that the data analysis accounted for the dead time correction correlation.

4.3 Backgrounds

4.3.1 Counting statistics ($\delta\dot{b}$)

Background measurement counting statistics are often combined with the counting statistics for the sample measurement and not presented separately. For high-resolution γ-ray detectors used in γ-spec and AA measurements, the backgrounds are the counts below the γ-ray photopeaks that are fit and subtracted out with peak fitting. The uncertainty in this process is usually incorporated into the counting statistics, but this should be avoided as this process induces correlations that are then neglected when the term "counting statistics" is used. No specific background uncertainty recommendations are provided for these sources as they vary strongly between experiments and even between data points.

4.3.2 Fitted backgrounds (δK or $\delta\dot{B}$)

For TAS and TED measurements, the background can be reported using equations (1) or (18). The background function is usually fit with a saturated resonance and a scattering sample, and with appropriate corrections, the uncertainty can be below 3%. If it is not documented that both a saturated resonance and scattering sample were used, an estimate of 3% is given in Table 1. The uncertainty δK is fully correlated between energy points within an experiment, as it is a constant factor. If the uncertainty $\delta\dot{B}$ is given instead, it is expected to have a strong Gaussian correlation across neutron energies, as it includes the correlated uncertainties and the counting statistics. Examples of detailed background analysis for TAS and TED can be found in references [50] and [67], respectively.

4.3.3 AMS "Reproducibility"

The AMS "reproducibility" uncertainty represents non-statistical fluctuations in the measured cross sections caused by many of the sources of background in AMS measurements. For experiments that require significant background suppression efforts, this uncertainty can be up to 10%, but if it is not clear that there were significant background suppression issues, 5% is a conservative estimate given in Table 2. This uncertainty depends on the ratio of target to product nuclei so it will be fully correlated between samples that were irradiated with the same neutron spectrum for the same amount of time, but in most cases, the reported data points will represent different neutron irradiations and it can be assumed to be

uncorrelated between the data points and between experiments. More details about this uncertainty source can be found in references [115,152].

4.4 Flux determination and normalization

4.4.1 Fluence ($\delta\Phi$)

In thermal spectrum-averaged and HER measurements, the fluence is typically determined using monitor reactions or the AP technique. There are many well-known reaction cross sections used for this purpose and typical uncertainties on the flux uncertainty are between 2% and 5%, which includes the "thermal equivalent" flux correction for epithermal neutrons. If no information is given about the flux normalization aside from the monitor reaction used, a value on the higher side is recommended in Table 2.

If possible, it is preferable to treat the sample and monitor measurements separately, as in the ratio in equation (14), and to estimate the uncertainty on each parameter or the ratio of parameters between the sample and monitor. For example, if the number density of the sample and monitor were measured with the same equipment, the uncertainties are highly correlated and the uncertainty on the ratio, $\delta(n_m/n_s)$, will be much smaller than the uncertainty on either value. If the measurement was not done in ratio and a flux estimate is needed, as is the case with AMS measurements that use AA for the flux determination, this template value should be used for the flux uncertainty in the absence of any specific flux uncertainty information.

If the AP technique is used, the uncertainty can be below 1%. If the uncertainty is not provided, an estimate between 1% and 3% is recommended based on how much information is known about the measurement. The uncertainty on $\delta\Phi$ is dependent on the efficiency for detecting the associated particle and the counting statistics achieved, so it can be much higher than the recommended 1%–3% range given in Table 2 in some cases.

Strong Gaussian correlations are expected between different data points in the same measurement, as the same neutron source and flux determination method are used. The same is expected between measurements at the same facility unless it is clear that different measurement methods were used, such as different monitor reactions. Weak correlations are expected between measurements if the only similarity is the nuclear data used for the reference reaction or neutron-production reaction, and no correlations are expected between measurements with different methods of flux characterization.

4.4.2 Flux ($\delta\phi$)

Direct measurement of the time-dependent flux is often done with fission chambers, but in-beam scintillators and long counters can also be used. These measurements have their own uncertainties based on the type of measurement, for which detailed descriptions of the uncertainties can be found in the appropriate templates–(n, f) template [9, 144] for fission chambers and (n, xn) template [157] for

other neutron detectors. If there is not enough information provided to allow for the use of those templates, a 3% uncertainty, at minimum, is recommended in Table 2.

Strong Gaussian correlations are recommended for data points within the same experiment due to the use of the same methods and reference data. Weak Gaussian correlations may be present between experiments using the same nuclear data for the fission chamber or in simulations of the neutron detector efficiencies, and for experiments using different measurement methods $\delta\phi$ can be assumed to be uncorrelated.

4.4.3 Flux normalization (δN_γ)

In resonance region TAS and TED measurements, the sample is typically measured in ratio to another resonance or isotope to allow for a flux normalization, N_γ, rather than a direct measurement. The uncertainty, δN_γ, accounts for uncertainty in the measurement of the reference and uncertainty in the relative efficiencies of the sample and the reference. It is reasonable for the reference measurement to have low statistical uncertainties around 1%, due to the use of a saturated resonance specifically chosen for the high capture yield. The most precise normalization values come from the use of a saturated resonance in the isotope being measured, known as an "internal" resonance. Typical uncertainties reported for internal resonance normalization are around 1%–2%. If there are no saturated resonances with the sample, a resonance in another isotope, an "external" resonance, can also be used. In this case, the efficiency of the system to detect capture events in the sample and reference material plays a large role in δN_γ, and values anywhere between 2% and 6% are reasonable. This uncertainty can be minimized by decreasing the sensitivity of the measurement to the cascade characteristics (with high efficiency in TAS and with a well-modeled cascade in the weighting function in TED) or by choosing a reference material with cascade characteristics very similar to the sample. Various studies of the PHWT used in TED measurements have shown external resonance normalization uncertainties within 2% [22,67,158], but these values rely on high precision γ-ray cascade models. Without specific information, uncertainty values at the low end of the 2%–6% range given in Table 1 are reasonable estimates if one of the following conditions is met: the reference material is known to have similar cascade characteristics to the sample, the efficiency of a TAS measurement is shown to be high enough that the cascade characteristics are unimportant, or the TED cascade model is shown to be accurate. Without enough information to determine such qualities, a value on the higher end is recommended.

δN_γ is fully correlated between energy points within the same dataset. Between experiments at the same facility using the same reference material, a moderate correlation is expected due to the same methods used. A weak or zero correlation is expected for experiments at different facilities and/or using different materials.

4.4.4 Beam fluctuation correction ($\delta\Delta\phi$)

The uncertainty on the beam fluctuation correction, $\delta\Delta\phi$ in equation (9), is usually negligible. The correction itself is small unless the half-life of the reaction product is comparable to the irradiation time, t_i, which is not commonly the case with product nuclei measured by AA, or in some cases when the counting time is comparable with the irradiation time. No recommended values are provided for $\delta\Delta\phi$, but it is expected to be fully correlated between data points in an experiment when it is significant.

4.5 Data analysis

4.5.1 AA times ($\delta t_i, \delta t_w, \delta t_c$)

The uncertainties on the irradiation, waiting, and counting times in equation (13) are usually negligible compared to other uncertainties in AA measurements. However, if the time or half-life uncertainties are not negligible, both sets of values are needed to propagate the uncertainties through equation (13) as detailed in reference [109].

Timing uncertainties are expected to be uncorrelated from each other (δt_i and δt_c are uncorrelated) but the use of the same time value for different samples can induce a correlation between data points. For example, if two samples are irradiated together, they will share the same t_i value and δt_i will be fully positively correlated between the two samples. The correlation induced by the time factor, f, should be calculated using equation (13).

4.5.2 CP angle-integration

In direct charged-particle measurements, the immediate experimental observable is the angle-differential reaction cross-section $\sigma_r(E_n, \theta)$. In many cases, the reported experimental result is the angle-integrated cross-section $\sigma_r(E_n)$ which contains additional uncertainty due to this integration.

One method is by fitting the measured $\sigma_r(E_n, \theta)$ to Legendre Polynomials and integrating over those functions. This process depends on assumptions about the outgoing angular distributions, and reported uncertainties vary widely–values as low as 0.2% and as high as 15% in the literature [98,153,159–161], depending on how well the distributions were believed to be known and on the solid-angle coverage. More information about the limitations of the available distributions can be found in reference [104].

4.5.3 Reference data

The uncertainties in reference data used in the analysis should not be estimated in general. If a citation is provided for the source of the data used, uncertainties reported in that reference should be used. If no uncertainties are given, deviations from current values should be considered. If no citation is given, contemporary libraries of the time (based on the publication year) can be used.

Branching ratios for reaction cascades, as used in γ-spectroscopy to convert from γ-transition cross sections, equation (6), to the reaction cross-section, are often calculated using reaction modeling codes. The uncertainty on individual calculated branching ratios and on the reaction cross-section inferred from the combination of multiple measured yields cannot be estimated in a general way [162,163] and more work is needed in this area before recommendations can be given.

4.5.4 Fluctuation correction (δF_γ)

The uncertainty on the fluctuation correction, δF_γ, for URR datasets is usually not reported. An estimate of this uncertainty should be based on specific information about the nuclear data used in the self-shielding and multiple scattering calculations, and no recommendation is given here. Reference [62] details measurements performed to validate self-shielding and can be used as a reference if this estimate is required. The correction is usually energy-dependent, and a strong Gaussian correlation is recommended. A strong correlation is expected between experiments using the same underlying nuclear data, and no correlation is expected otherwise.

5 Conclusions

This work presents a template of expected measurement uncertainties for measurements of neutron-induced capture and charged-particle production cross-sections. The in-beam measurements covered are Total Absorption Spectroscopy, Total Energy Detection, γ-ray Spectroscopy, and direct charged-particle measurement. The offline measurements covered are Activation Analysis and Accelerator Mass Spectroscopy. Recommended uncertainty values and correlations are provided for uncertainty sources where estimation is reasonable. Some uncertainty sources are difficult to estimate without detailed knowledge of the experiment and data analysis, such as the overall efficiency uncertainties for TAS and TED measurements and the resolution function uncertainty. Recommendations may be possible in the future with further studies on realistic ranges of these uncertainties for older measurements.

Conflict of interests

The authors declare that they have no competing interest to report.

Data availability statement

The data that were created associated with this manuscript are all within its main text and tables.

Author contribution statement

A.M. Lewis: writing – original draft. D. Neudecker: writing – original draft. A.D. Carlson: writing – original draft. D.L. Smith: writing – original draft. I. Thompson: writing – original draft. A. Wallner: writing – original draft. D.P. Barry: writing – review and editing. L.A. Bernstein: writing – review and editing. R.C. Block: writing – review and editing. S. Croft: writing – review and editing. Y. Danon: writing – review and editing. M. Drosg: writing – review and editing. R.C. Haight: writing – review and editing. M.W. Herman: writing – review and editing. H.Y. Lee: writing – review and editing. N. Otuka: writing – review and editing. H. Sjöstrand: writing – review and editing. V. Sobes: writing – review and editing.

References

1. H. Farrar, et al., Helium production cross section of boron for fast reactor neutron spectra, Nucl. Technol. **25**, 305 (1975)
2. Y. Danon, et al., Simultaneous measurement of ^{235}U fission and capture cross sections from 0.01 eV to 3 keV using a gamma multiplicity detector, Nucl. Sci. Eng. **187**, 291 (2017)
3. M. Heil, et al., A neutron source to measure stellar neutron capture cross sections at $kT = 5$ keV, Nucl. Phys. A **758**, 529 (2005)
4. C. Lederer-Woods, et al., Destruction of the cosmic γ-ray emitter ^{26}Al in massive stars: Study of the key ^{26}Al(n, p) reaction, Phys. Rev. C **104**, l022803 (2021)
5. A. Wallner, et al., AMS–A powerful tool for probing nucleosynthesis via long-lived radionuclides, Eur. Phys. J. A **27**, 337 (2006)
6. Z. Rvay, et al., Cold neutron PGAA facility at Budapest, Nucl. Instrum. Meth. B **213**, 385 (2004)
7. E.A. Mackey, et al., New thermal neutron prompt γ-ray activation analysis instrument at the National Institute of Standards and Technology Center for Neutron Research, Nucl. Instrum. Meth. B **226**, 426 (2004)
8. D. Neudecker, et al., Templates of expected measurement uncertainties, EPJ Nuclear Sci. Technol. **9**, 35 (2023)
9. D. Neudecker, et al., Applying a Template of Expected Uncertainties to Updating ^{239}Pu(n,f) Cross-section Covariances in the Neutron Data Standards Database, Nucl. Data Sheets **163**, 228 (2020)
10. A.M. Lewis, Uncertainty Analysis Procedures for Neutron-Induced Cross Section Measurements and Evaluations, Ph.D. thesis, University of California, Berkeley, Department of Nuclear Engineering, 2020
11. A.D. Carlson, et al., Fluctuations in neutron total cross sections, Phys. Rev. **158**, 1142 (1967)
12. R. Policroniades, et al., An associated particle time-of-flight facility for neutron cross section measurement, Nucl. Instrum. Meth. A **346**, 230 (1994)
13. E.M. Hafner, et al., The Total n-p Scattering Cross Section at 4.75 Mev, Phys. Rev. **89**, 204 (1953)
14. A. Bratenahl, et al., Neutron total cross sections in the 7- to 14-Mev region, Phys. Rev. **110**, 927 (1958)
15. D.B. Fossan, et al., Neutron total cross sections of Be, B^{10}, B, C, and O, Phys. Rev. **123**, 209 (1961)
16. G.D. Kim, et al., Production of monoenergetic MeV-range neutrons by ^{3}H(p,n)^{3}He reaction, J. Radioanal Nucl. Chem. **271**, 541 (2007)
17. I. Slypen, et al., Light charged particle emission induced by fast neutrons with energies between 25 and 65 MeV on iron, J. Phys. G **30**, 45 (2004)
18. K. Wisshak, et al., The Karlsruhe 4π barium fluoride detector, Nucl. Instrum. Meth. A **299**, 60 (1990)
19. D.G. Schuster, Production of collimated monoenergetic beams of neutrons from 2 MeV to 14 MeV by the associated particle method, Nucl. Instrum. Meth. **76**, 35 (1969)
20. H. Vonach, et al., Przisionsmessung des ^{27}Al(n,α)-Wirkungsquerschnitts fr 14,43 MeV-Neutronen, Z. Phys. **237**, 155 (1970)
21. C. Guerrero, et al., Performance of the neutron time-of-flight facility n_TOF at CERN, Eur. Phys. J. A **49**, 27 (2013)
22. P. Schillebeeckx, et al., Determination of resonance parameters and their covariances from neutron induced reaction cross section data, Nucl. Data Sheets **113**, 3054 (2012)
23. A. Wallner, et al., Stellar and thermal neutron capture cross section of ^{9}Be, Phys. Rev. C **99**, 1 (2019)
24. B.J. McDermott, et al., ^{181}Ta(n,γ) cross section and average resonance parameter measurements in the unresolved resonance region from 24 to 1180 keV using a filtered-beam technique, Phys. Rev. C **96**, 014607 (2017)
25. M. Bhike, et al., Neutron-capture cross-section measurements of ^{136}Xe between 0.4 and 14.8 MeV, Phys. Rev. C **89**, 031602 (2014)
26. J.A. Becker, et al., New Physics Opportunities with GEANIE at LANSCE/WNR, Nucl. Phys. News **7**, 11 (1997)
27. C. Rouki, et al., High resolution measurement of neutron inelastic scattering cross-sections for ^{23}Na, Nucl. Instrum. Meth. A **672**, 82 (2012)
28. D.A. Brown, et al., ENDF/B-VIII.0: The 8th major release of the nuclear reaction data library with CIELO-project cross sections, new standards and thermal scattering Data, Nucl. Data Sheets **148**, 1 (2018)
29. A.J. Plompen, et al., The joint evaluated fission and fusion nuclear data library, JEFF-3.3, Eur. Phys. J. A **56**, 1 (2020)
30. O. Iwamoto, et al., Japanese evaluated nuclear data library version 5: JENDL-5, J. Nucl. Sci. Technol. **60**, 1 (2023)
31. A. Trkov, et al., IRDFF-II: A new neutron metrology library, Nucl. Data Sheets **163**, 1 (2020)
32. M.R. Bhat, Evaluated Nuclear Structure Data File (ENSDF), in *Nuclear Data for Science and Technology*, Research Reports in Physics, (Springer Berlin Heidelberg, 1992), pp. 817–821
33. A.M. Lewis, et al., Templates of expected measurement uncertainties for total cross section observables, EPJ Nuclear Sci. Technol. **9**, 34, (2023)

34. P.A. Moldauer, Evaluation of the fluctuation enhancement factor, Phys. Rev. C **14**, 764 (1976)

35. R.C. Block, et al., A multiplicity detector for accurate low-energy capture measurement, in *Proceedings of Nuclear Data for Science and Technology 1988*, JEARI, Mito, Japan, 1988

36. B.C. Diven, et al., Radiative capture cross sections for fast neutrons, Phys. Rev. **120**, 556 (1960)

37. K. Wisshak, et al., Neutron capture in ^{148,150}Sm: A sensitive probe of the *s*-process neutron density, Phys. Rev. C **48**, 1401 (1993)

38. K.H. Guber, et al., A BaF$_2$ detector system for (n,γ) cross section measurements at ORELA, Nucl. Phys. A **621**, 254 (1997)

39. S. Yamamoto, et al., Application of BGO scintillators to absolute measurement of neutron capture cross sections between 0.01 eV and 10 eV , J. Nucl. Sci. Technol. **33**, 815 (1996)

40. K. Kobayashi, et al., Neutron capture cross-section measurement of ^{99}Tc by linac time-of-flight method and the resonance analysis, Nucl. Sci. Eng. **146**, 209 (2004)

41. C. Guerrero, et al., The n_TOF total absorption calorimeter for neutron capture measurements at CERN, Nucl. Instrum. Meth. A **608**, 424 (2009)

42. P.W. Lisowski, et al., The los alamos national laboratory spallation neutron sources, Nucl. Sci. Eng. **106**, 208 (1990)

43. R.C. Block, et al., Neutron radiative capture measurements utilizing a large liquid scintillator detector at the ORNL fast chopper, in *Proceedings of the International Conference on Time of Flight Methods*, Saclay, France, 1961

44. R. Reifarth, et al., Background identification and suppression for the measurement of (n,γ) reactions with the DANCE array at LANSCE, Nucl. Instrum. Meth. A **531**, 530 (2004)

45. C. Guerrero, et al., Monte Carlo simulation of the n_TOF Total Absorption Calorimeter, Nucl. Instrum. Meth. A **671**, 108 (2012)

46. S. Agostinelli, et al., GEANT4 a simulation toolkit, Nucl. Instrum. Meth. A **506**, 250 (2003)

47. T. Burrows, Nuclear Data Sheets for A = 49, Nucl. Data Sheets **109**, 1879 (2008)

48. J. Balibrea, et al., Measurement of the neutron capture cross section of the ^{235}U with the CERN n_TOF total absorption calorimeter and a fission tagging based on micromegas detectors, Nucl. Data Sheets **119**, 10 (2014)

49. A. Laminack, et al., Measurement of neutron-capture cross sections of ^{70,72}Ge using the DANCE facility, Phys. Rev. C **106**, 025802 (2022)

50. K. Wisshak, et al., Measurements of keV neutron capture cross sections with a 4π barium fluoride detector: Examples of ^{93}Nb, ^{103}Rh, and ^{181}Ta, Phys. Rev. C **42**, 1731 (1990)

51. D.P. Barry, et al., Neutron transmission and capture measurements and resonance parameter analysis of neodymium from 1 to 500 eV, Nucl. Sci. Eng. **153**, 8 (2006)

52. R.C. Block, et al., Neutron transmission and capture measurements and analysis of Dy from 0.01 to 550 eV, Prog. Nucl. Energy **94**, 126 (2017)

53. C.J. Prokop, et al., Measurement of the ^{65}Cu(n,γ) cross section using the detector for advanced neutron capture experiments at LANL, Phys. Rev. C **99**, 055809 (2019)

54. K. Wisshak, et al., Stellar neutron capture cross section of the unstable s-process branching point ^{151}Sm, Phys. Rev. C **73**, 015802 (2006)

55. F. Voss, et al., Stellar neutron capture cross sections of Pr and Dy isotopes, Phys. Rev. C **59**, 1154 (1999)

56. J.L. Ullmann, et al., The detector for advanced neutron capture experiments: A 4π BaF$_2$ detector for neutron capture measurements at LANSCE, AIP Conf. Proc. **769**, 918 (2005)

57. A. Borella, et al., Determination of the ^{232}Th(n,γ) cross section from 4 to 140 keV at GELINA, Nucl. Sci. Eng. **152**, 1 (2006)

58. G. Aerts, et al., Neutron capture cross section of ^{232}Th measured at the n_TOF facility at CERN in the unresolved resonance region up to 1 MeV, Phys. Rev. C **73**, 1 (2006)

59. K. Kobayashi, et al., Measurement of neutron capture cross section of ^{237}Np by LINAC Time-of-Flight Method and with Linac-driven Lead Slowing-down Spectrometer, J. Nucl. Sci. Technol. **39**, 111 (2002)

60. P.E. Koehler, et al., High-resolution neutron capture and transmission measurements, and the stellar neutron-capture cross section of ^{88}Sr, Phys. Rev. C **62**, 15 (2000)

61. A. Kimura, et al., Current activities and future plans for nuclear data measurements at J-PARC, Eur. Phys. J. A **51**, 180 (2015)

62. J.M. Brown, et al., Validation of unresolved neutron resonance parameters using a thick-sample transmission measurement, Nucl. Sci. Eng. **194**, 221 (2020)

63. M. Moxon, et al., A gamma-ray detector for neutron capture cross-section measurements, Nucl. Instrum. Meth. **24**, 445 (1963)

64. R.L. Macklin, et al., Capture-cross-section studies for 30–220 keV neutrons using a new technique, Phys. Rev. **159**, 1007 (1967)

65. C. Domingo-Pardo, i-TED: A novel concept for high-sensitivity (n,γ) cross-section measurements, Nucl. Instrum. Meth. A **825**, 78 (2016)

66. V. Babiano-Surez, et al., Imaging neutron capture cross sections: i-TED proof-of-concept and future prospects based on Machine-Learning techniques, Eur. Phys. J. A **57**, 197 (2021)

67. A. Borella, et al., The use of C6D6 detectors for neutron induced capture cross-section measurements in the resonance region, Nucl. Instrum. Meth. A **577**, 626 (2007)

68. R.E. Chrien, et al., The Brookhaven High Flux Beam Reactor fast chopper facility, Nucl. Instrum. Meth. **53**, 93 (1967)

69. V. Bondarenko, et al., Nuclear structure of ^{157}Gd, Nucl. Phys. A **726**, 175 (2003)

70. T. Belgya, Prompt gamma activation analysis at the budapest research reactor, Phys. Procedia **31**, 99 (2012)

71. H.D. Choi, et al., *Database of Prompt Gamma Rays from Slow Neutron Capture for Elemental Analysis* (Vienna, IAEA, 2007)

72. F.F. Arbocc, et al., Experimental determination of k_0, Q_0, $\bar{E}_r$ factors and neutron cross-sections for 41 isotopes of interest in Neutron Activation Analysis, J. Radioanal Nucl. Chem. **296**, 931 (2013)

73. C.J. Werner, et al., MCNP Users Manual – Code Version 6.2, Tech. rep., LA-UR-17-29981, 2017

74. E. Gete, et al., Neutron-induced peaks in Ge detectors from evaporation neutrons, Nucl. Instrum. Meth. A **388**, 212 (1997)

75. N. Fotiades, et al., Measurements and calculations of ^{238}U(n,xnγ) partial γ-ray cross sections, Phys. Rev. C **69**, 024601 (2004)

76. R.B. Firestone, et al., Thermal neutron capture cross section for ^{56}Fe(n,γ), Phys. Rev. C **95**, 1 (2017)

77. F. Bev, Simulation of γ cascades in complex nuclei with emphasis on assessment of uncertainties of cascade-related quantities, Nucl. Instrum. Meth. A **417**, 434 (1998)

78. L.E. Kirsch, et al., RAINIER: A simulation tool for distributions of excited nuclear states and cascade fluctuations, Nucl. Instrum. Meth. A **892**, 30 (2018)

79. D. Jordan, et al., An event generator for simulations of complex β-decay experiments, Nucl. Instrum. Meth. A **828**, 52 (2016)

80. P.G. Young, et al., Comprehensive nuclear model calculations: Introduction to the theory and use of the GNASH code, Tech. rep., LA-12343-MS, 1992

81. M. Herman, et al., EMPIRE: Nuclear reaction model code system for data evaluation, Nucl. Data Sheets **108**, 2655 (2007)

82. T. Kawano, et al., Monte Carlo simulation for particle and γ-ray emissions in statistical Hauser-Feshbach model, J. Nucl. Sci. Technol. **47**, 462 (2010)

83. A.J. Koning, et al., Modern nuclear data evaluation with the TALYS code system, Nucl. Data Sheets **113**, 2841 (2012)

84. L.A. Bernstein, et al., ^{239}Pu(n,2n)^{238}Pu cross section deduced using a combination of experiment and theory, Phys. Rev. C **65**, 216011 (2002)

85. T.N. Massey, et al., Charged-particle emission in neutron reactions on ^{10}B, Phys. Rev. C **105**, 054612 (2022)

86. H.Y. Lee, et al., ^{16}O(n,α) cross section investigation using LENZ instrument at LANSCE, EPJ Web Conf. **122**, 05004 (2016)

87. F.J. Hambsch, et al., The ^{10}B(n,α_0)/^{10}B(n,$\alpha_1\gamma$) branching ratio, Nucl. Sci. Eng. **156**, 103 (2017)

88. G. Zhang, et al., Measurement of differential and angle-integrated cross sections of the ^{6}Li(n,t)^{4}He reaction in the MeV neutron energy range, Nucl. Instrum. Meth. A **566**, 615 (2006)

89. P.E. Koehler, et al., Two detectors for (n,p) and (n,α) measurements at white neutron sources, Nucl. Instrum. Meth. A **361**, 270 (1995)

90. C. Romano, et al., Measurements of (n,α) cross-section of small samples using a lead-slowing-down-spectrometer, Nucl. Instrum. Meth. A **562**, 771 (2006)

91. S.M. Grimes, et al., Charged-particle-producing reactions of 15-MeV neutrons on ^{51}V and ^{93}Nb, Phys. Rev. C **17**, 508 (1978)

92. L. Cosentino, et al., Experimental setup and procedure for the measurement of the ^{7}Be(n,α)α reaction at n_TOF, Nucl. Instrum. Meth. A **830**, 197 (2016)

93. C. Weiβ, et al., The (n,α) reaction in the s-process branching point ^{59}Ni, Nucl. Data Sheets **120**, 208 (2014)

94. P. Kavrigin, et al., ^{13}C(n,α_0)^{10}Be cross section measurement with sCVD diamond detector, Eur. Phys. J. A **52**, 179 (2016)

95. D.B. Gayther, A measurement of the ^{6}Li(n,α) cross-section, Ann. Nucl. Energy **4**, 515 (1977)

96. W.P. Poenitz, Measurements of the ^{6}Li(n,α)T cross section in the keV energy range, Zeitschrift fr Physik **268**, 359 (1974)

97. S. Carboni, et al., Particle identification using the technique and pulse shape discrimination with the silicon detectors of the FAZIA project, Nucl. Instrum. Meth. A **664**, 251 (2012)

98. H. Jiang, et al., Measurements of differential and angle-integrated cross sections for the ^{10}B(n,α)^{7}Li reaction in the neutron energy range from 1.0 eV to 2.5 MeV, Chin. Phys. C **43**, 124002 (2019)

99. A. Badal, et al., Trends in particle and nuclei identification techniques in nuclear physics experiments, La Rivista del Nuovo Cimento **45**, 189 (2022)

100. J.B. England, et al., Z-identification of charged particles by signal risetime in silicon surface barrier detectors, Nucl. Instrum. Meth. A **280**, 291 (1989)

101. S.A. Kuvin, et al., Direct measurement of ^{59}Ni(n,p)^{59}Co and ^{59}Ni(n,α)^{56}Fe at fast-neutron energies from 500 keV to 10 MeV, Phys. Rev. C **105**, 044608 (2022)

102. S.A. Kuvin, et al., Nonstatistical fluctuations in the ^{35}Cl(n,p)^{35}S reaction cross section at fast-neutron energies from 0.6 to 6 MeV, Phys. Rev. C **102**, 024623 (2020)

103. M. Drosg, Corrections for neutron source cross section data measured by proton-recoil counter telescopes in the presence of water-spray cooling of the source, Tech. rep., INDC(AUS)-0022, 2020

104. H.I. Kim, et al., New evaluation on angular distributions and energy spectra for neutron-induced charged-particle measurements, Nucl. Instrum. Meth. A **963**, 163699 (2020)

105. F. Marie, et al., Thermal neutron capture cross-section measurements of ^{243}Am and ^{242}Pu using the new mini-INCA α- and γ-spectroscopy station, Nucl. Instrum. Meth. A **556**, 547 (2006)

106. S. Bisterzo, et al., Measurement of the ^{209}Bi(n,γ)^{210}Bi^g cross section and updated s-process analysis of the Pb/Bi region, in *Proceedings of the International Conference on Nuclear Data for Science and Technology*, Les Ulis, France, 2007, pp. 2–5

107. L. Weissman, et al., Measurement of ^{208}Pb(n,γ)^{209}Pb Maxwellian averaged neutron capture cross section, Phys. Rev. C **96**, 1 (2017)

108. C. Goessling, et al., Experimental study of ^{113}Cd β decay using CdZnTe detectors, Phys. Rev. C **72**, 4 (2005)

109. N. Otuka, et al., Uncertainty propagation in activation cross section measurements, Radiat. Phys. Chem. **140**, 502 (2017)

110. G.J. McCallum, et al., Influence of source-detector distance on relative intensity and angular correlation measurements with Ge(Li) spectrometers, Nucl. Instrum. Meth. **130**, 189 (1975)

111. A.N. Berlizov, et al., Software for X- and gamma-ray spectrometry, J. Radioanal Nucl. Chem. **264**, 169 (2005)

112. D.L. Smith, et al., Measurement of the ^{51}V(n,p)^{51}Ti Reaction Cross Section from Threshold to 9.3 MeV by the Activation Method, Tech. rep., ANL/NDM-85, 1984

113. D.W. Kneff, et al., Experimental and theoretical determination of helium production in copper and aluminum by 14.8-MeV neutrons, Nucl. Technol. **49**, 498 (1980)

114. W. Kutschera, et al., Accelerator mass spectrometry in nuclear physics and astrophysics, Ann. Rev. Nucl. Part. Sci. **40**, 411 (1990)

115. A. Wallner, et al., AMS measurements of ^{41}Ca and ^{55}Fe at VERA – two radionuclides of astrophysical interest, Nucl. Instrum. Meth. B **259**, 677 (2007)

116. C.Y. Chen, et al., Ultrasensitive isotope trace analyses with a magneto-optical trap, Science **286**, 1139 (1999)

117. M. Tessler, et al., Stellar r-process neutron capture cross sections on determined via activation, atom trap trace analysis, and decay counting, Phys. Rev. C **104**, 015806 (2021)

118. H. Nassar, et al., Stellar (n, γ) cross section of ^{62}Ni, Phys. Rev. Lett. **94**, 7 (2005)

119. I. Dillmann, et al., Determination of the stellar (n,γ) cross section of ^{40}Ca with accelerator mass spectrometry, Phys. Rev. C **79**, 1 (2009)

120. P. Steier, et al., VERA, an AMS facility for "all" isotopes, Nucl. Instrum. Meth. B **223-224**, 67 (2004)

121. A. Wallner, et al., Novel Method to Study Neutron Capture of ^{235}U and ^{238}U Simultaneously at keV Energies, Phys. Rev. Lett. **112**, 192501 (2014)

122. M. Paul, et al., Heavy ion separation with a gas-filled magnetic spectrograph, Nucl. Instrum. Meth. A **277**, 418 (1989)

123. M. Schlapp, et al., A new 14 GHz electron-cyclotron-resonance ion source for the heavy ion accelerator facility ATLAS, Rev. Sci. Inst. **69**, 631 (1998)

124. H. Nagai, et al., Measurements of ^{10}Be and ^{26}Al in some meteorites with internal beam monitor method, Nucl. Instrum. Meth. B **29**, 266 (1987)

125. C. Stan-Sion, et al., AMS measurement of the neutron capture cross-section ^{209}Bi(n, $γ)^{210m}$Bi, Nucl. Instrum. Meth. B **259**, 739 (2007)

126. G. Rugel, et al., Measurement of (n,γ) reaction cross sections at stellar energies for ^{58}Ni and ^{78}Se, Nucl. Instrum. Meth. B **259**, 683 (2007)

127. L.K. Fifield, Accelerator mass spectrometry and its applications, Rep. Prog. Phys. **62**, 1223 (1999)

128. H.-A. Synal, Developments in accelerator mass spectrometry, Int. J. Mass Spec. **349–350**, 192 (2013)

129. W. Kutschera, Applications of accelerator mass spectrometry, Int. J. Mass Spec. **349–350**, 203 (2013)

130. A. Wallner, et al., High-sensitivity isobar-free AMS measurements and reference materials for ^{55}Fe, ^{68}Ge and ^{202g}Pb, Nucl. Instrum. Meth. B **294**, 374 (2013)

131. A. Wallner, et al., Settling the half-life of ^{60}Fe: Fundamental for a versatile astrophysical chronometer, Phys. Rev. Lett. **114**, 1 (2015)

132. A. Arazi, et al., Measurement of ^{25}Mg(p,γ)^{26g}Al resonance strengths via accelerator mass spectrometry, Phys. Rev. C **74**, 1 (2006)

133. A.M. Lane, et al., R-matrix theory of nuclear reactions, Rev. Mod. Phys. **30**, 257 (1958)

134. N.M. Larson, Updated Users Guide for SAMMY: Multilevel R-Matrix Fits to Neutron Data Using Bayes' Equations, Tech. rep., ORNL/TM-9179/R8, 2008

135. M.C. Moxon, et al., GEEL REFIT, A least squares fitting program for resonance analysis of neutron transmission and capture data computer code, Tech. rep., AEA-InTec-0630, 1991

136. G. M. Hale, Use of R-matrix methods for light element evaluations, in *Proceedings of the Conference on Nuclear Data Evaluation Methods and Procedures* (Brookhaven National Laboratory, Upton, NY, 1981), p. 509

137. G.M. Hale, et al., Data covariances from R-matrix analyses of light nuclei, Nucl. Data Sheets **123**, 165 (2015)

138. C.W. Reich, et al., Multilevel formula for the fission process, Phys. Rev. **111**, 929 (1958)

139. W. Hauser, et al., The inelastic scattering of neutrons, Phys. Rev. **87**, 366 (1952)

140. B. Becker, et al., Analysis of Geel Spectra – AGS, Tech. rep., NEA/DB/DOC(2014)4, 2014

141. B. Becker, et al., Data reduction and uncertainty propagation of time-of-flight spectra with AGS, J. Inst. **7**, P11002 (2012)

142. N. Otuka, et al., Towards a more complete and accurate experimental nuclear reaction data library (EXFOR): International collaboration between nuclear reaction data centres (NRDC), Nucl. Data Sheets **120**, 272 (2014)

143. F. Gunsing, et al., EXFOR Data in Resonance Region and Spectrometer Response Function, Tech. rep., INDC(NDS)-0647, 2012

144. D. Neudecker, et al., Template for estimating uncertainties of measured neutron-induced fission cross-sections, EPJ Nuclear Sci. Technol. **4**, 21 (2018)

145. G. Leinweber, et al., Neutron capture and total cross-section measurements and resonance parameters of gadolinium, Nucl. Sci. Eng. **154**, 261 (2006)

146. P. Žugec, et al., Experimental neutron capture data of ^{58}Ni, Phys. Rev. C **89**, 014605 (2014)

147. Y. Danon, et al., Fission cross-section measurements of ^{247}Cm, ^{254}Es, and ^{250}Cf from 0.1 eV to 80 keV, Nucl. Sci. Eng. **109**, 341 (1991)

148. R.C. Block, et al., Neutron transmission and capture measurements of ^{133}Cs from 600 to 2000 eV, Nucl. Sci. Eng. **195**, 679 (2021)

149. M.J. Trbovich, et al., Hafnium resonance parameter analysis using neutron capture and transmission experiments, Nucl. Sci. Eng. **161**, 303 (2009)

150. W. Ratynski, et al., Neutron capture cross section of ^{197}Au: A standard for stellar nucleosynthesis, Phys. Rev. C **37**, 595 (1988)

151. V. Semkova, et al., Uncertainties of calculated coincidence-summing correction factors in gamma-ray spectrometry, EPJ Web Conf. **239**, 12003 (2020)

152. A. Wallner, et al., Precise measurement of the thermal and stellar ^{54}Fe(n,γ)^{55}Fe cross sections via accelerator mass spectrometry, Phys. Rev. C **96**, 025808 (2017)

153. H. Bai, et al., Measurement of the differential cross sections and angle-integrated cross sections of the ^{6}Li(n,t)^{4}He reaction from 1.0 eV to 3.0 MeV at the CSNS Back-n white neutron source, Chin. Phys. C **44**, 014003 (2020)

154. M. Drosg, et al., Calibration of a Li-glass detector for neutron energies above 50 keV by the ^{1}H(t,n)^{3}He reaction, Nucl. Instrum. Meth. B **94**, 319 (1994)

155. L.C. Mihailescu, et al., Investigations for the use of the fast digitizers with detectors for radiative capture measurements at GELINA, Nucl. Instrum. Meth. A **600**, 453 (2009)

156. M.S. Moore, Rate dependence of counting losses in neutron time-of-flight measurements, Nucl. Instrum. Meth. **169**, 245 (1980)

157. J.R. Vanhoy, et al., Templates of expected measurement uncertainties for (n,xn) cross sections, EPJ Nuclear Sci. Technol. **9**, 31 (2023)

158. N. Yamamuro, et al., Reliability of the weighting function for the pulse height weighting technique, Nucl. Instrum. Meth. **133**, 531 (1976)

159. R.C. Haight, et al., Charged-particle emission in reactions of 15-MeV neutrons with ^{89}Y, ^{90}Zr, and ^{92,94,95,96}Mo, Phys. Rev. C **23**, 700 (1981)

160. S.M. Grimes, et al., Charged-particle emission in reactions of 15-MeV neutrons with isotopes of chromium, iron, nickel, and copper, Phys. Rev. C **19**, 2127 (1979)

161. S. Kunieda, et al., Measurement and model analysis of (n,xα) cross sections for Cr, Fe, ^{59}Co, and ^{58,60}Ni from threshold energy to 150 MeV, Phys. Rev. C **85**, 054602 (2012)

162. M. Kerveno, et al., How to produce accurate inelastic cross sections from an indirect measurement method?, EPJ Nuclear Sci. Technol. **4**, 23 (2018)

163. A.M. Lewis, et al., Ratio method for estimating uncertainty in calculated gamma cascades, Eur. Phys. J. A **55**, 141 (2019)